Geochemistry Geophysics Geosystems G3
AN ELECTRONIC JOURNAL OF THE EARTH SCIENCES
Published by AGU and the Geochemical Society

Article
Volume 8, Number 11
24 November 2007
Q11008, doi:10.1029/2007GC001675
ISSN: 1525-2027

Multiple hydrothermal sources along the south Tonga arc and Valu Fa Ridge

Gary Massoth
GNS Science, P.O. Box 30-328, Lower Hutt, New Zealand

Now at Mass-Ex3 Consulting LLC, 2100 Lake Washington Boulevard N, N101, Renton, Washington 98056, USA (gary.massoth@gmail.com)

Edward Baker
NOAA Pacific Marine Environmental Laboratory, 7600 Sand Point Way NE, Seattle, Washington 98115, USA

Tim Worthington
Institute of Geosciences, University of Kiel, Olshausenstrasse 40, D-24118 Kiel, Germany

John Lupton
NOAA Pacific Marine Environmental Laboratory, 2115 SE O.S.U. Drive, Newport, Oregon 97365-5258, USA

Cornel de Ronde
GNS Science, P.O. Box 30-368, Lower Hutt, New Zealand

Richard Arculus
Australian National University, Canberra, ACT 0200, Australia

Sharon Walker
NOAA Pacific Marine Environmental Laboratory, 7600 Sand Point Way NE, Seattle, Washington 98115, USA

Ko-ichi Nakamura
National Institute of Advanced Industrial Science and Technology, AIST Tsukuba Central 7, 1-1-1 Higashi, Tsukuba, Ibarake, 305-8567, Japan

Jun-ichiro Ishibashi
Department of Earth and Planetary Sciences, Kyushu University, Hakozaki, Higashi-ku, Fukuoka 812-8581, Japan

Peter Stoffers
Institute of Geosciences, University of Kiel, Olshausenstrasse 40, D-24118 Kiel, Germany

Joseph Resing
JISAO/University of Washington, 7600 Sand Point Way NE, Seattle, Washington 98115, USA

Ronald Greene
CIMRS/Oregon State University, 2115 SE O.S.U. Drive, Newport, Oregon 97365, USA

Geoffrey Lebon
JISAO/University of Washington, 7600 Sand Point Way NE, Seattle, Washington 98115, USA

[1] Quantifying hydrothermal venting at the boundaries of tectonic plates is an outstanding geoscience problem. Considerable progress has been made by detailed surveys along mid-ocean ridges (MORs), but until recently little was known about fluid venting along volcanic arcs. We present the first systematic survey for hydrothermal venting along the 425-km-long south Tonga arc and new chemistry data for particle and thermal plumes previously reported along an adjacent 88-km-long section of the back-arc Valu Fa Ridge (VFR). Eleven hydrothermal plumes, recognized by their anomalous light backscattering, Eh, temperature, pH, dissolved ^{3}He, CH_4, and total dissolvable Fe and Mn, were identified arising from seven volcanic centers along the arc. Five plumes on the VFR were characterized chemically. Vent field density for the south Tonga arc was 2.6 sites/100 km of arc front, comparable to that found by surveys of the Kermadec arc (1.9 to 3.8 sites/100 km) and to MORs in the eastern Pacific (average value for 2280 km of surveyed ridgecrest: 3.2 sites/100 km). A ''vent gap'' occurs along a 190 km section of the arc closest to the VFR, and a site density twice the average for MORs on the eastern edge of the Pacific plate was found on this part of the VFR (6.6 sites/100 km). We suggest magmas ascending under the adjacent south Tonga arc have been captured by the VFR. While chemical enrichments of plumes on the south Tonga arc were, in general, slightly less than those on the Kermadec arc, several instances of excessive anomalies in pH suggest a similar presence of fluids enriched in magmatic volatiles (CO_2-SO_2-H_2S). Locally, venting on the VFR has contributed to accumulations of ^{3}He, Fe, and Mn within the southern Lau basin. On a broader scale, our results provide considerable support for the notion that venting from intraoceanic arcs on the convergent margin of the Pacific plate adds significantly to the total hydrothermal input into the Pacific Ocean.

Components: 13,222 words, 18 figures, 3 tables.

Keywords: Intraoceanic; arc; back arc; hydrothermal; plume.

Index Terms: 3017 Marine Geology and Geophysics: Hydrothermal systems (0450, 1034, 3616, 4832, 8135, 8424); 3060 Marine Geology and Geophysics: Subduction zone processes (1031, 3613, 8170, 8413); 3001 Marine Geology and Geophysics: Back-arc basin processes.

Received 2 May 2007; **Revised** 24 August 2007; **Accepted** 29 August 2007; **Published** 24 November 2007.

Massoth, G., et al. (2007), Multiple hydrothermal sources along the south Tonga arc and Valu Fa Ridge, *Geochem. Geophys. Geosyst.*, *8*, Q11008, doi:10.1029/2007GC001675.

1. Introduction

[2] Systematic reconnaissance surveys for hydrothermal venting conducted during the last ~20 a have covered ~25% (~2280 km) of the mid-ocean ridge (MOR) spreading centers along the eastern edge of the Pacific plate and revealed an average of 3.2 vent sites per 100 km of ridge crest [*Baker and German*, 2004]. More recently, hydrothermal surveys have commenced along the submerged volcanic arcs of the western Pacific formed in response to subduction of the Pacific plate. The general distribution of hydrothermal activity along ~60% of this arc front (~3800 km of ~6400 km total length), chiefly the Mariana and Tonga-Kermadec arcs, has now been established [*de Ronde et al.*, 2001, 2003, 2007; *Embley et al.*, 2004; *Massoth et al.*, 2005]. First results from surveys along southern and mid-Kermadec and Mariana arc sections suggest a spatial density of venting similar to that on MORs [*de Ronde et al.*, 2001, 2007; *Baker et al.*, 2003; *Embley et al.*, 2004], and that in many cases the hydrothermal fluids are highly enriched in acid volatiles (e.g., CO_2 and sulfur gases) and Fe compared to hydrothermal fluids venting from MORs [*de Ronde et al.*, 2001; *Massoth et al.*, 2003; *Embley et al.*, 2006; *Lupton et al.*, 2006]. Here we report the details of the first systematic survey of venting along the south Tonga (Tofua) arc, a 425-km-long segment of the ~2530-km-long Tonga-Kermadec subduction system (Figures 1 and 2).

[3] The south Tonga arc is one of several worldwide where a back-arc spreading center closely approaches (≤110 km) an active volcanic front (others include the north Tonga arc, the Bismarck arc, and the terminations of the Mariana and South Sandwich arcs [*Martinez and Taylor*, 2003]). In this setting, the back-arc segments closest to the

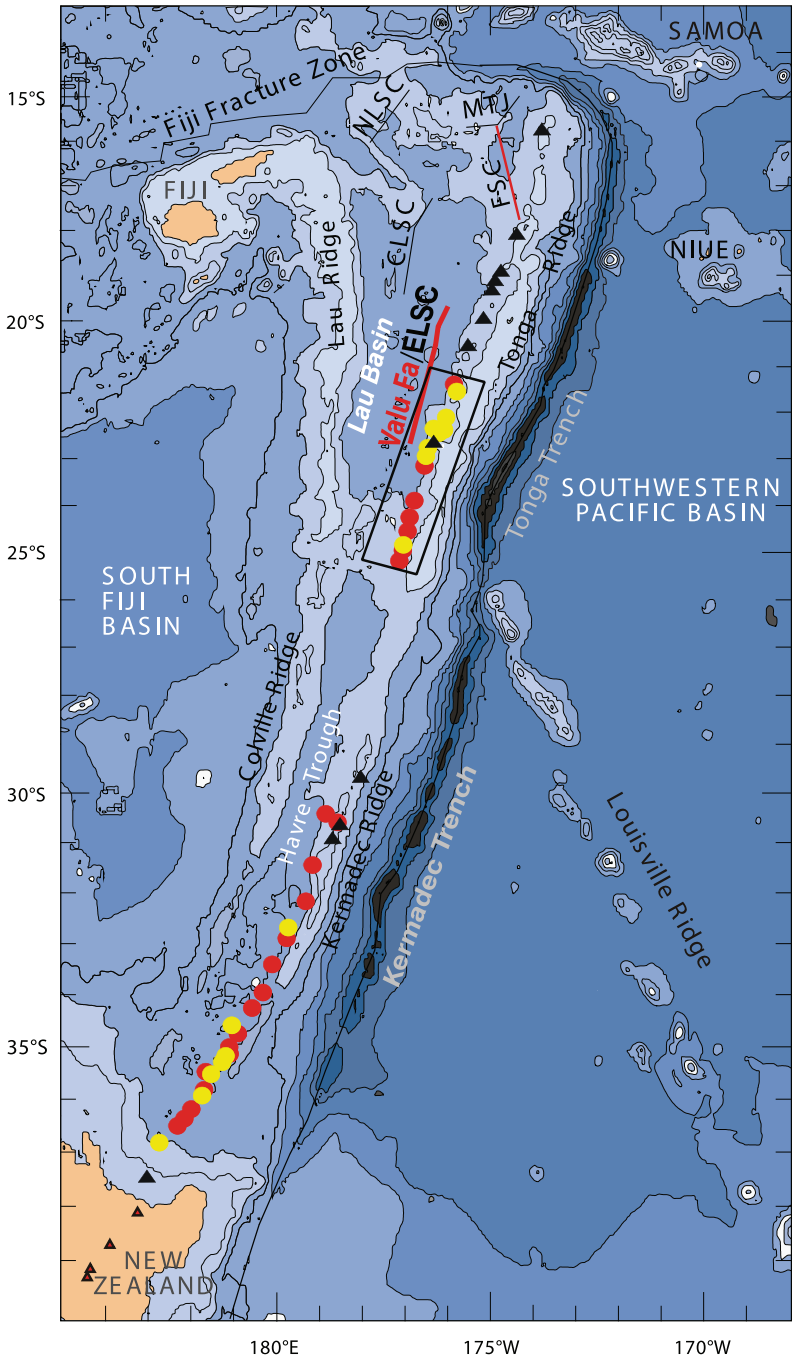

Figure 1. Tonga-Kermadec subduction system. The Pacific plate subducts westward beneath the Australian plate along the Tonga and Kermadec trenches, setting the global speed record for subduction (24 cm/a) near 16°S [*Bevis et al.*, 1995] and creating the deepest point in the southern hemisphere at ~23°15′S (Horizon Deep, 10,866 m depth [*Wright et al.*, 2000]). The ~2530-km-long Tonga-Kermadec intraoceanic arc lies 165–230 km west of the trench axes and ~100 km above the subducted slab. Including the *TELVE* (2003) study area (outlined by black box), 37 submarine volcanic centers have been surveyed along one half (1265 km) of the active Tonga-Kermadec arc front. Volcanic centers with plume evidence for seafloor venting are shown as red circles, and others are shown as yellow circles; the 12 volcanic islands along the arc front are indicated by black triangles. Details of the preceding NZAPLUME I (1999) and II (2002) surveys along the Kermadec arc south of 30°S have been previously reported [*de Ronde et al.*, 2001, 2007; *Baker et al.*, 2003; *Massoth et al.*, 2003]. MTJ is the Mangatolu Triple Junction from which the Fonualei Spreading Center (FSC) approaches the North Tonga arc.

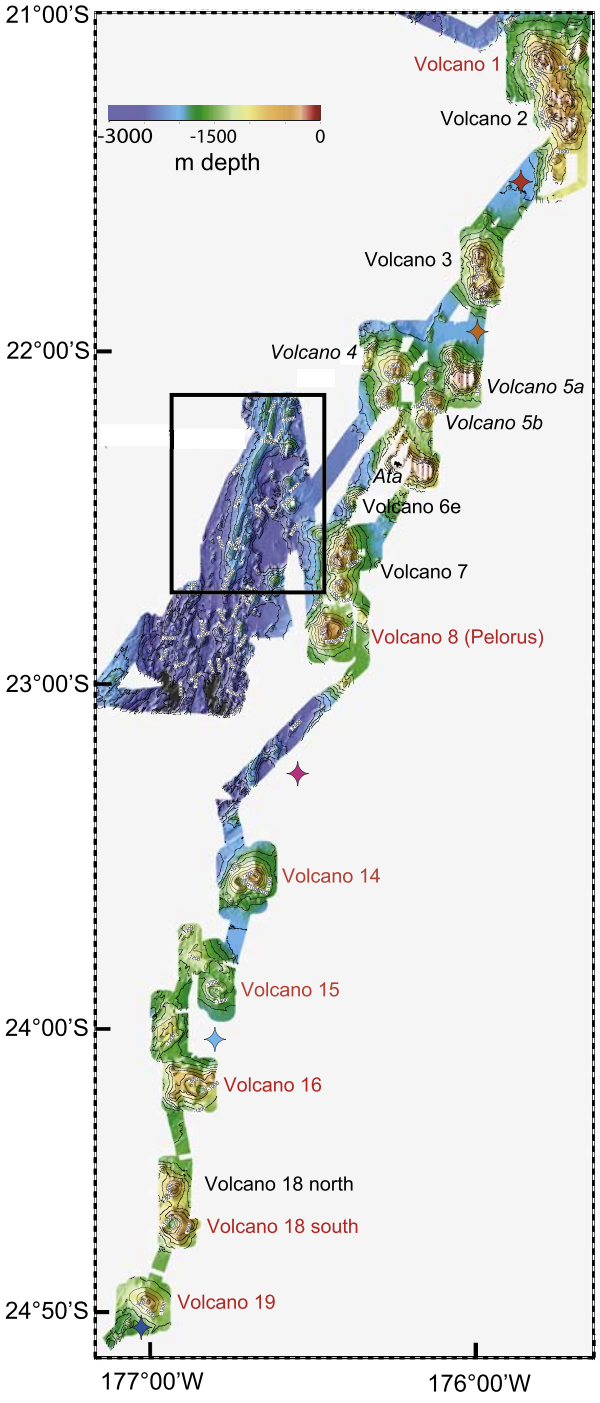

Figure 2. South Tonga (Tofua) arc and Valu Fa back-arc (enclosed box) regions surveyed for venting during *TELVE*. Bathymetry and names for the 15 major volcanic centers along the 425-km-long arc front are from SO-167 [*Stoffers et al.*, 2003]. Center names in red indicate plume evidence for venting. Ata, located adjacent to the Valu Fa survey region, is the only subaerial volcano of the South Tonga arc. The five color-filled stars along the arc front mark off-site, "background" water sampling stations discussed in the text.

volcanic front commonly exhibit magmatic inflation, enhanced magma generation and an arc-like geochemical signature in their lavas [e.g., *Martinez and Taylor*, 2002, 2003; *Taylor and Martinez*, 2003]. In contrast, the more distant back-arc regions have MOR-like tectonic and magmatic characteristics. To investigate whether hydrothermal fluids from back-arc centers proximal to volcanic arcs are influenced by an arc component, we also surveyed the southern 88 km of the Valu Fa Ridge (VFR) for hydrothermal plumes (Figures 1–3). The VFR is the segment of the Eastern Lau Spreading Center (ELSC) closest (~ 40 km) to the volcanic front [*Zellmer and Taylor*, 2001]. Particle and thermal plumes mapped along the VFR during this and subsequent surveys have been reported elsewhere [*Baker et al.*, 2005, 2006; *Martinez et al.*, 2006].

[4] Our plume surveys were conducted during the March–April 2003 *TELVE* (Tonga-Eastern Lau Vents Expedition) cruise of the R/V *Southern Surveyor*. *TELVE* augmented previous plume surveys along the southern and mid-Kermadec arcs (NZAPLUME I and II) [*de Ronde et al.*, 2001, 2007; *Baker et al.*, 2003; *Massoth et al.*, 2003]. Figure 1 provides an overview of the volcanic centers that have been surveyed along the Tonga-Kermadec arc and indicates (in red) those with evidence for active seafloor venting.

2. Setting

2.1. South Tonga Arc

[5] The Tonga-Kermadec subduction system (Figure 1) is the longest on Earth, extending over ~2530 km in length, comprising ~40% of the intraoceanic arc front in the western Pacific [*de Ronde et al.*, 2003]. Magmatic activity along this tectonic margin is localized as insular volcanic centers, which sometimes can be complex morphologically due to polygenetic volcanism. Following the convention of *Cañón-Tapia and Walker* [2004], to include all volcanic constructs clustered within an ~10 km diameter as a single volcanic system, ~60 submarine volcanic centers comprise the full arc front. Our focus here is on the 425-km-long segment between 21°–25°S, which we refer to as the south Tonga arc (Figure 2). This arc segment lies ~180 km west of the Tonga Trench, where oceanic crust of mid-Cretaceous age is subducting at ~165 mm/a [*Bevis et al.*, 1995]. The volcanic front is built upon the western margin of the Tonga Ridge, a remnant Eocene arc capped by a 3- to 4-km-thick carbonate platform with interbedded volcan-

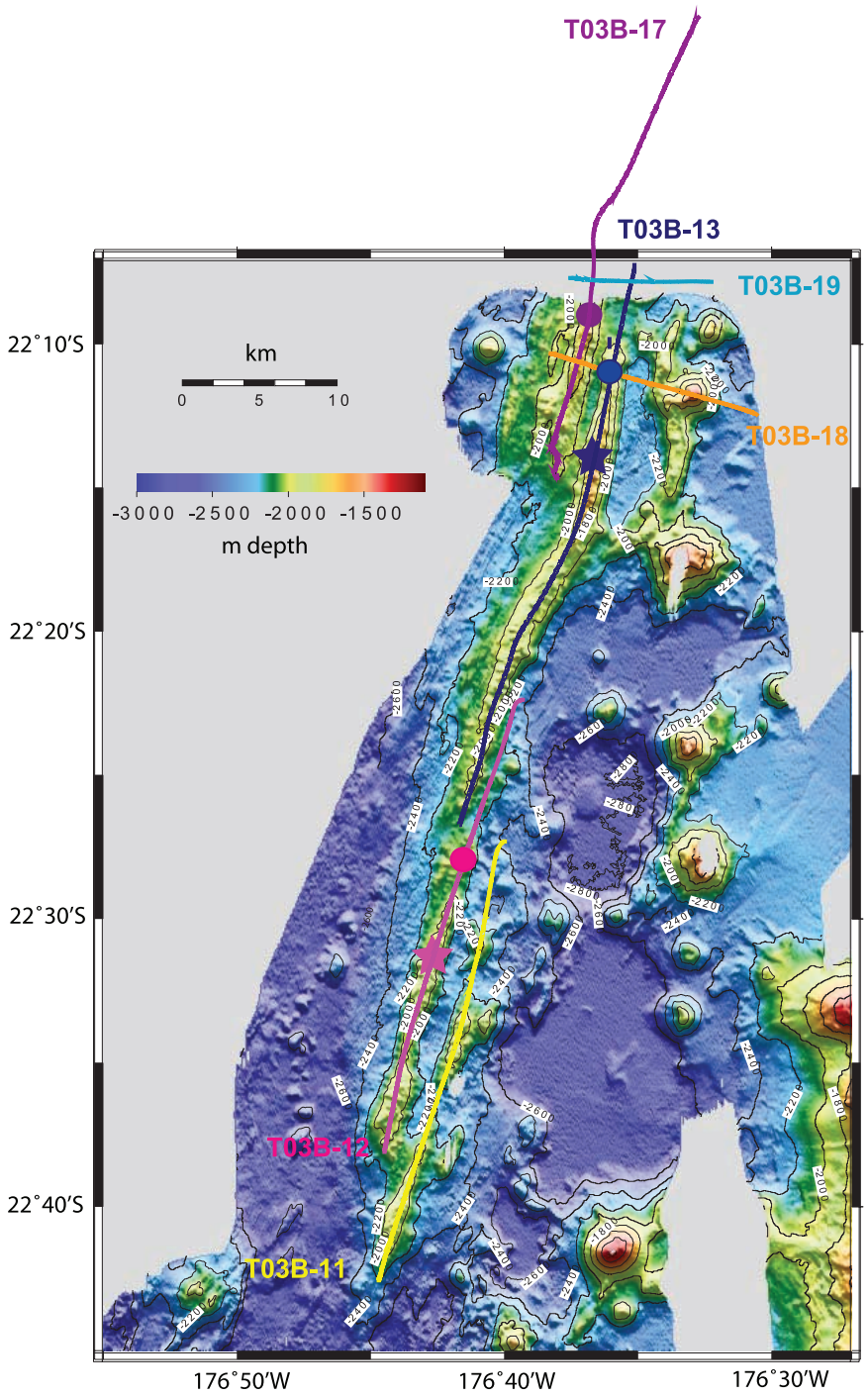

Figure 3. Southern reach of the Valu Fa back-arc spreading ridge mapped during SO-167. Towpaths along the Southern (yellow and magenta), Central (blue), and Northern (purple) VFR ridgecrests (terminology of *Wiedicke and Collier* [1993]) and across the overlap region near 22°10′S are shown. Historic vent sites Hine Hina and Vai Lili are marked by magenta and blue stars on the Southern and Central VFR segments, respectively. Circles at the northern tips of these ridgecrests and at the southern end of the Northern ridge mark the centers of the Misiteli (magenta), Mariner (blue), and TELVE (purple) plumes.

istic sediments [*Bloomer et al.*, 1994; *Hawkins*, 1995]. Lavas of the volcanic front range from basalt to rhyolite (predominantly basaltic andesite), and can be classified as a low-K series that exhibits the classic subduction signature of strong enrichment in the large ion lithophile elements (e.g., Rb, Ba, Sr, Pb) relative to MOR basalts (T. Worthington et al., manuscript in preparation, 2007). Ferromanganese crusts of predominantly hydrothermal origin have been recovered from the south Tonga arc [*Hein et al.*, 1990], but hydrothermal plumes have not previously been reported.

[6] Multibeam mapping of the south Tonga arc was completed during the SO-167 cruise of the F/S *Sonne* [*Stoffers et al.*, 2003]. Fifteen submarine volcanic centers (averaging one per 28 km of arc length) including 27 major volcanic constructs were identified and sampled along a 40-km-wide corridor between 21°09′ and 24°48′S (Figure 2) (T. Worthington et al., manuscript in preparation, 2007). Our *TELVE* cruise utilized the SO-167 bathymetry to complete a comprehensive survey for vent plumes above most of the volcanic constructs. Subsequently, a diving campaign using the PISCES submersibles has further examined the active fields discovered in the summit calderas of Volcanoes 1 and 19 (Figure 2) [*Stoffers et al.*, 2006].

2.2. Valu Fa Ridge

[7] The VFR extends 152 km between 21°26′ and 22°44′S and is the southernmost segment of the ELSC (Figure 1) [*Martinez et al.*, 2006]. It consists of three overlapping, left-offset ridge crests at 1600–2000 m depth (Southern, Central, and Northern), and can be further subdivided into 11 higher-order segments [*von Stackelberg and the Shipboard Scientific Party*, 1988; *Wiedicke and Collier*, 1993]. Spreading rates decrease from 61 to 39 mm/a as the VFR converges from ~60 to within ~40 km of the South Tonga arc [*Zellmer and Taylor*, 2001]. Seismic imaging provides strong evidence for a magma lens ~3.2 km beneath the Central VFR [*Morton and Sleep*, 1985; *Collier and Sinha*, 1990, 1992], which may be continuous beneath much of the VFR [*Harding et al.*, 2000]. Seismic tomography suggests this melt lens thins toward the Central VFR segment center, consistent with the idea that the overlapping spreading center between the Central and Northern VFR segments is currently a site of enhanced magmatism [*Turner et al.*, 1999; *Day et al.*, 2001]. Lavas recovered from the VFR range from basalt to rhyolite and are characterized by a distinct arc-like geochemical signature (e.g., high Ba/La and H_2O) that contrasts with the more MORB-like compositions erupted along the northern ELSC at greater distances from the south Tonga arc [*Taylor and Martinez*, 2003, and references therein]; the more silicic compositions are irregularly distributed along the VFR.

[8] A series of surveys along the VFR-ELSC beginning in the mid-1980s culminated with the discovery of the Hine Hina (40°C, ~1900 m, Southern VFR), Vai Lili (342°C, ~1720 m, Central VFR) and the inactive White Church hydrothermal fields [*Fouquet et al.*, 1991a, 1991b, 1993]. The Hine Hina and Vai Lili fields were further investigated using deep-towed video and thermal sensors during the SO-167 cruise [*Stoffers et al.*, 2003; *Fretzdorff et al.*, 2006]. Subsequently, our *TELVE* cruise re-surveyed the southernmost 88 km (60%) of the VFR including all of the Southern and Central segments together with part of the Northern segment (Figure 3; ridge sections V3–V10 of *Wiedicke and Collier* [1993]). Since then, water column plume and multibeam/acoustic imaging surveys of the full ELSC have been completed [*Martinez et al.*, 2006; *Baker et al.*, 2006]. Also, the submersible *Shinkai 6500* revisited the Hine Hina and Vai Lili vent sites together with the Mariner field [*Ishibashi et al.*, 2006] in 2004 followed by several ROV *Jason* dive campaigns [e.g., *Tivey et al.*, 2005; *Seewald et al.*, 2005; *Sharkey et al.*, 2005] part of the RIDGE 2000 Integrated Study Site activities focused in this region. The first evidence for the existence of the Mariner field came from the detection of the overlying water column plume during *TELVE* [*Baker et al.*, 2005].

3. Methods

[9] Our plume reconnaissance relied on real-time sensing of conductivity-temperature-depth-optical light scattering-Eh (CTD-O-Eh) during vertical casts and tow-yos [e.g., *Baker et al.*, 2002, 2005]. We deployed a Sea Bird 911plus CTD/rosette system fitted with sensors for optical light backscattering (Sea Point LBSS and Wet Labs models were deployed in tandem) and Eh and Niskin-style water sampling bottles. While temperature anomalies ($\Delta\theta$) have been reported for VFR plumes [*Baker et al.*, 2005, 2006], estimating $\Delta\theta$ within South Tonga arc plumes was difficult due to hydrographic masking associated with steep gradients in temperature and density at these more shallow sites (Figure 4). Voltage outputs from the

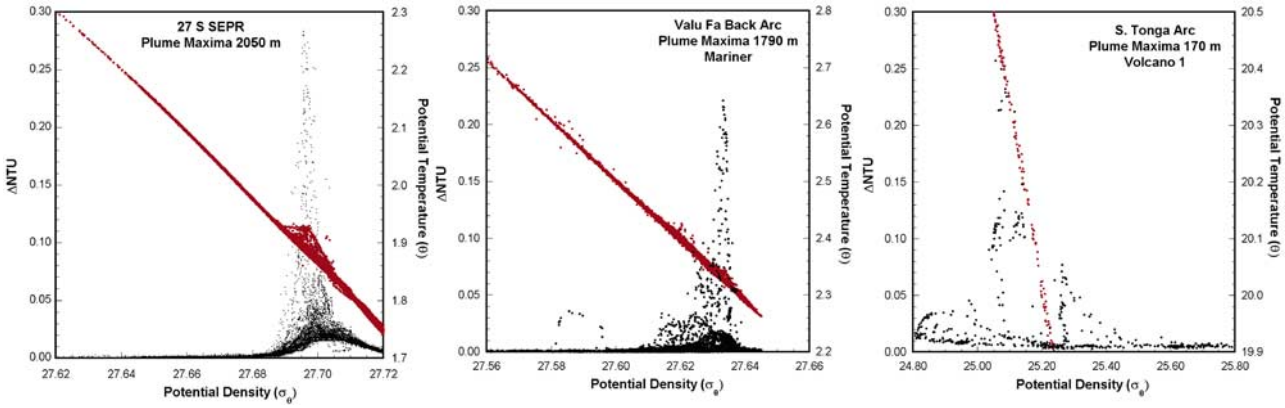

Figure 4. Type examples of potential temperature (θ)–potential density (σ_θ) relations (red data points) for plumes at (left) Pacific MORs (superfast spreading East Pacific Rise at 27°S), (middle) back-arc ridges (Mariner site on VFR), and (right) generally shallow arc volcanoes (Volcano 1, South Tonga arc). Light backscattering anomaly data (as ΔNTU, black data points) are shown as additional markers of the plumes. High gradients in $\Delta\theta/\Delta\sigma_\theta$ common at shallow arc venting depths preclude clear resolution of thermal anomalies (seen as positive deviations from the regional trends for the MOR and back-arc examples) within arc plumes. Density stratification ($\Delta\sigma_\theta/\Delta Z$, seafloor-to-plume top) for the MOR and back-arc sites shown (12×10^{-5} and 3.5×10^{-5} kg/m^4, respectively) is an order of magnitude less than at non-enclosed venting sites on the South Tonga arc ($100-725 \times 10^{-5}$ kg/m^4). This translates into a similar "order-of-magnitude" effect on the rise heights of plumes in these settings: e.g., plume maxima were located ~180 m above vents at the Mariner site on the VFR (vent field depth from *Ishibashi et al.* [2006]) and ~20 m above vents on the summits of Volcanoes 1 and 19 (vent field depth from *Stoffers et al.* [2006]).

backscattering sensors were normalized to nephelometric turbidity units (NTUs, a dimensionless optical standard) according to the procedures of *Baker et al.* [2001], with ΔNTUs being unit values above ambient seawater. Relative Eh voltages in the range −0.5 to +0.5 V were measured between a Pt electrode in seawater and a Ag-AgCl reference electrode in saturated KCl solution [*Tachibana et al.*, 1991].

[10] Seawater samples for helium determinations were cold-weld sealed in Cu tubing using a hydraulic press [*Young and Lupton*, 1983]. Samples for CH_4 determinations were preserved with $HgCl_2$, crimp-sealed in glass, and refrigerated in darkness pending analysis. Samples were drawn into glass syringes and plastic bottles for shipboard determinations of dissolved H_2S and pH, respectively. Unfiltered samples were collected in acid-cleaned polyethylene bottles and acidified to pH 1.6 for determinations of total dissolvable Mn (TDMn) and Fe (TDFe). Particulates were captured on acid-cleaned 0.4 μm pore diameter poly carbonate membranes using closed-system, nitrogen overpressure filtration. The membranes were rinsed with pH ~8 DI water and stored un-desiccated.

[11] Determinations of H_2S were made soon after sample collection using flow-injection analysis and colorimetric detection sensitive above 300 nM [*Sakamoto-Arnold et al.*, 1986]. An Orion Ross combination electrode was used to determine pH on samples thermally equilibrated in a water bath. Stable output voltages under gentle stirring were referenced to NBS standards to assign pH values with a replicate precision of ±0.005 pH units and a detection limit for anomalies in pH of 0.01–0.02 pH units.

[12] Isotope ratios and concentrations of helium were determined at the NOAA/PMEL Helium Isotope Laboratory in Newport, OR USA using a 21-cm-radius mass spectrometer with 1σ precision of 0.2% for ^{3}He/^{4}He ratios and an accuracy of 1% for the absolute He concentration. Methane was determined with ±5% precision at Kyushu University, Japan using an automated analysis system described by *Ishibashi et al.* [1997] based on purge-and-trap gas separation and GC-FID detection. Manganese and Fe were determined at GNS Science in New Zealand using flow-injection analyses and colorimetric detection following the methods of *Resing and Mottl* [1992] (modified by adding 4 g of nitriloacetic acid/L of buffer) and *Measures et al.* [1995], respectively. Nominal precision for the Mn determination was ≤6% and for Fe ≤8%. Particulate sulfur (PS) and manganese (PMn) were determined at NOAA/PMEL in Seattle, WA, USA using thin-film secondary emission x-ray

fluorescence [*Feely et al.*, 1991] with analytical precisions of 11% and 1%, respectively.

4. Results

4.1. South Tonga Arc

[13] Site surveys for hydrothermal plumes were completed at 20 of the 27 major volcanic constructs (basal diameters of 10–25 km, summits 1000–2000 m above the seafloor) discovered during SO-167 (Figure 2). The volcanoes that were not surveyed were clearly inactive (heavily sedimented or topographically degraded). Tow-yo deployments were carried out at most sites in preference to vertical casts in order to maximize coverage of the complex volcanic edifices, with towpaths often crossing small cones and craters on a single pass. Hydrothermal plumes were detected at seven volcanic centers (1, 8, 14, 15, 16, 18S and 19; Figure 2), four of which had plumes arising from multiple sites (1, 8, 18S, and 19). Thus 11 plumes were detected in total. Below we describe the physical parameters monitored in real-time during tow-yos and vertical casts (optical light scattering and Eh) and the chemical parameters determined at sea and ashore (dissolved gases: He, CH_4, H_2S, and pH as proxy indicator of CO_2 and sulfur gases; the two most abundant metals commonly found in vent fluids: Fe and Mn; and PMn and PS, particulate manganese and sulfur).

4.1.1. Volcano 1

[14] This major stratovolcano is capped by an oval caldera 7 km long by 4.5 km wide (Figure 5). Two post-caldera scoria cones on the SW caldera rim rise to ~100 mbsl, while the deepest parts of the caldera are at ~450 mbsl. Towpaths crossed the enclosed southern reach of the caldera and three quadrants surrounding each of the scoria cones (Figure 5, left panel). Two distinct particle plumes were mapped as ΔNTU (Figure 5, right panels): a thin (~20 m) plume with a maximum at 170 m depth was located near the southern cone, and a thicker (80+ m) plume with lower values of ΔNTU reaching a maximum at ~400 m depth within the southern caldera. The Eh voltage measured along the towpath showed strong negative deflections (indicating more reducing conditions) in association with the shallow plume, but not for the deep plume. The numerical values for the respective plume maxima in ΔNTU and ΔEh (taken as the departure from the ambient signal) here and at the other arc sites are given in Table 1. It can be seen that the shallow plume at Volcano 1 had the highest values found anywhere on the south Tonga arc.

[15] Although our chemical results are derived from samples collected along saw-tooth-shaped towpaths with greater horizontal dimension than vertical (e.g., Figure 5), nevertheless we present our chemical data for the active sites as vertical profiles. Figures 6 and 7 show vertical profiles for CH_4 and δ^3He (where $\delta^3\text{He} = 100[(R/R_A) - 1]$, $R = {}^3\text{He}/{}^4\text{He}$ and R_A is the ratio for air) and for TDFe and TDMn, respectively. This presentation style is consistent with our ability to focus sampling on discrete plume maxima using real-time signals from our in situ sensors. Table 1 lists maximum values at each site for these chemical plume tracers (including δ^3He in excess of the depth-variable regional value), plus ΔpH, particulate sulfur and manganese, along with mean values for Fe/Mn. The shallow plume at Volcano 1 had the highest δ^3He, CH_4, and ΔpH values on the south Tonga arc and a significant enrichment in Fe. The deep plume at this site also had a large ΔpH anomaly, a high Fe concentration and elevated levels of PS and PMn compared to most of the sites sampled. The Fe/Mn value for this plume (5.4 ± 0.6) was twice that of most other sites.

4.1.2. Volcano 8

[16] Also known as Pelorus Reef, this is a large but simple stratocone (Figure 8). A circular caldera, ~5 km in diameter, forms the summit and is largely infilled by post-caldera volcanism along its western margin. Water-depths at the summit range from 35 mbsl (western summit) to 500 mbsl within the caldera. Two particle plumes were detected during a single tow-yo. The ΔNTU intensities of both plumes were about half the magnitude of the deep plume at Volcano 1 (Figure 8 and Table 1). A 50-m-thick plume layer centered at 240 m depth bordered the northeast wall of Volcano 8, while a thinner plume layer with maxima at 440 m resided within the NW caldera and possibly beyond the caldera wall. Anomalies in Eh were not discernable above background (Figure 8). While no anomaly in δ^3He, and low levels of TDMn (background concentration ~2 ± 1 nM) were detected at this site, the particle plumes here were associated with distinct anomalies in ΔpH and Fe, and the upper plume had a slightly elevated CH_4 concentration (the deeper plume was not sampled).

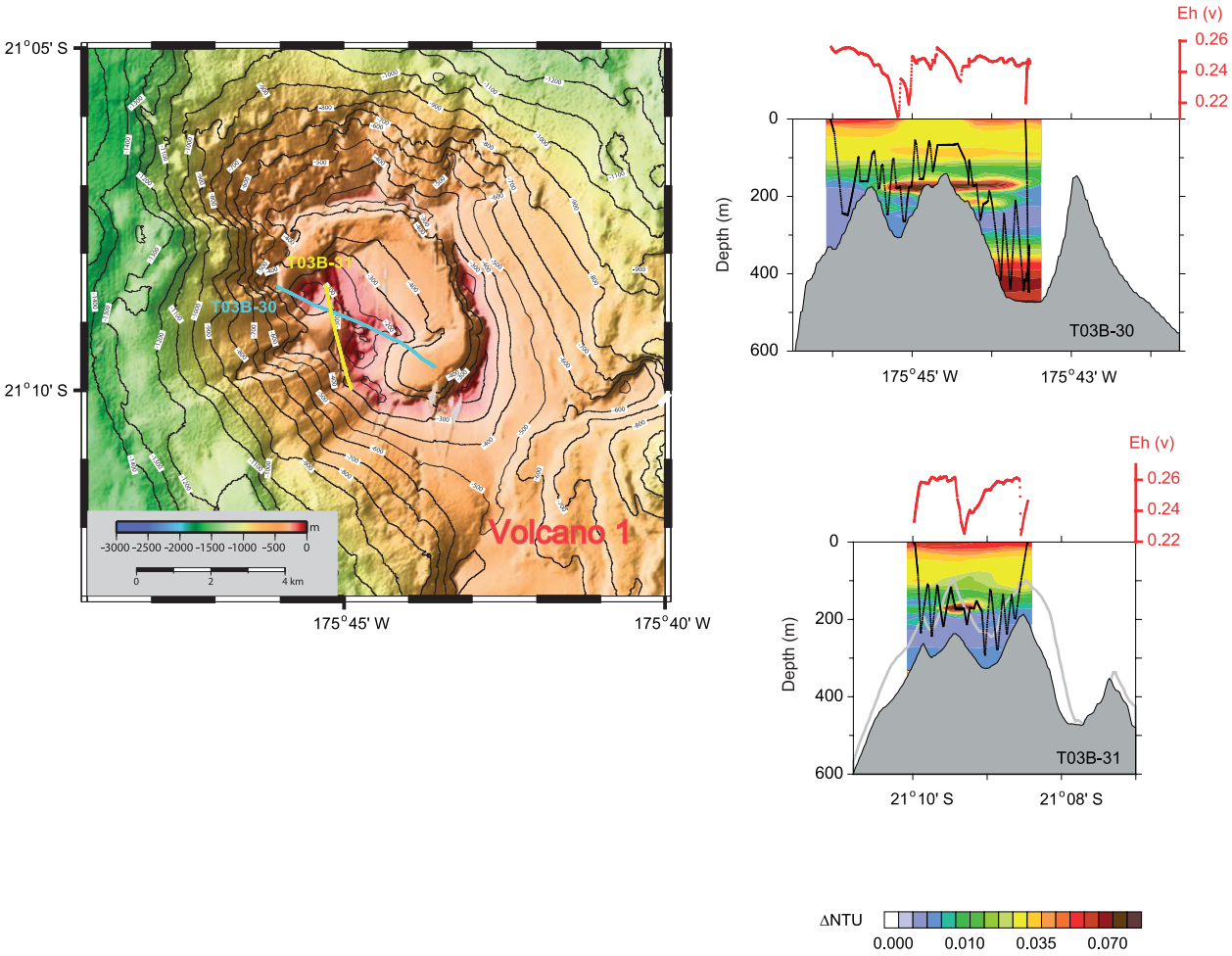

Figure 5. Plan view of bathymetry and towpaths (left-hand panel) and cross-section views of towpaths and light backscattering plume distributions, expressed as ΔNTU units (right-hand panels), at Volcano 1. Relative voltages recorded by the Eh sensor along the towpaths are shown above the plume maps (note: the large deflections at the beginnings and/or ends of some records are artifacts induced by deployment/recovery operations). Raised bathymetric profile shown as a gray line for tow T03B-31 (bottom right panel) depicts minimum depths along the summit ridge slightly east of the towpath. The sill depth of the caldera is given in Table 1. The light-scattering layer that extends from the surface to about 200 m depth is a regional biogenic-detrital feature.

4.1.3. Volcano 14

[17] The twin cones of Volcano 14, both capped by small summit calderas, rise to a minimum depth of 480 mbsl (Figure 9). A single particle plume, centered at 985 m depth, was detected within the 640-m-deep western caldera. Plume intensity along the towpath was highest near the eastern wall of this caldera, where the signal magnitude was less than half that observed at Volcano 8 (Table 1). Discernable anomalies in Eh were not observed. Moderate chemical anomalies in ^{3}He, CH_4, ΔpH, Fe, and Mn were found at plume depth, with lesser, uniform values below that indicating mixing within the enclosed caldera (Figures 6 and 7 and Table 1).

4.1.4. Volcano 15

[18] With a height of just over 700 m (summit at 1080 mbsl), Volcano 15 is one of the smaller edifices surveyed (Figure 10). Evidence of a weak particle plume was seen within a 150-m-deep crater that is itself nested within a small summit caldera. While the significant changes in Eh and pH associated with the particle plume suggest it is hydrothermal, the very small anomalies measured for ^{3}He, Fe, and Mn provide only weak support for this conclusion (Figures 6 and 7 and Table 1).

4.1.5. Volcano 16

[19] The complex, irregularly shaped Volcano 16 features three summit peaks at 550 to 750 mbsl that

Table 1. Plume Maxima at Sites Along the South Tonga Arc and Valu Fa Back Arc

Site	Rock Assoc.[a]	Plume, m	Sill, m	ΔNTU	ΔEh V_{rel}	ΔpH	δ^3He,[b] %	δ^3He Anom.[c]	CH_4 nM,	TDFe, nM	TDMn, nM	Fe/Mn,[d] mol/mol	PS, nM	PMn, nM
S. Tonga Arc														
Vol. 1 SW Cone	BA-A	170		0.318	−0.05	−0.08	73	75	7.1	101	29	2.5 ± 0.5	7	0.3
Vol. 1 Caldera	BA-A	400	>400	0.084	−0.01	−0.07	24	24	5.2	118	20	5.4 ± 0.6	21	4.8
Vol. 8 NW Wall	B-A	240		0.049	nd[e]	−0.02	−0.3	0	3.2	26	1	nd	nd	0.5
Vol. 8 Caldera	BA	440	>400	0.035	nd	−0.04	1.9	0	–[f]	60	4	nd	–	–
Vol. 14 Caldera	B-R	985	850	0.015	nd	−0.03	42	35	4.6	68	51	1.1 ± 0.3	0.2	0.7
Vol. 15 Crater	B	1340	1350	0.006	−0.02	−0.03	26	2	–	8	9	1.3 ± 1.1	–	–
Vol. 16 Crater	A-R	1340	950	0.044	nd	nd	24	17	5.8	9	9	0.8 ± 0.4	18	0.7
Vol. 18S E Cone	BA	305		0.100	−0.02	−0.05	43	42	4.3	227	12	18.8	6	0.4
Vol. 18S Caldera	R	890	950	0.027	−0.01	nd	37	30	6.1	137	52	1.8 ± 0.4	nd	5.9
Vol. 19 Summit	B-BA	385		0.015	nd	nd	18	18	3.5	48	36	1.2 ± 0.3	0.2	0.4
Vol. 19 Caldera	B-BA	875	820	0.098	−0.02	−0.03	45	40	3.5	310	108	3.0 ± 0.2	0.3	4.7
Valu Fa Back Arc														
Hine Hina	BA	1890		0.001	nd	−0.01	39	0	1.7	21	13	1.2 ± 0.2	–	–
Vai Lili	A	1710		0.002	−0.01	−0.03	39	3	3.6	77	126	1.2 ± 0.4	–	–
Misiteli	R	1860		0.016	−0.02	−0.02	46	8	3.5	30	37	0.9 ± 0.3	12	2.2
Mariner	B-D	1735		0.219	−0.07	−0.04	57	20	3.7	812	197	2.0 ± 0.8	195	3.3
TELVE	B-A	1650		0.028	−0.03	−0.02	50	15	3.4	96	147	1.2 ± 0.4	–	–

[a] Rock Association refers to range of rock fractionation recovered from the seafloor surface beneath the respective plumes: basalt (B) to basaltic andesite (BA) to andesite (A) to dacite (D) to rhyolite (R); data for S. Tonga arc are from SO-167 dredge samples (T. Worthington, unpublished data, 2003) and for Valu Fa back arc are for lavas collected during *TELVE* (D. Christie and C. Goddard, personal communication, 2006).
[b] The isotopic abundance of ^{3}He is expressed in percent as δ^3He(= 100[(R/R_A) − 1], where R is the ratio ^{3}He/^{4}He in the sample and air).
[c] "δ^3He Anom." is the increase in the δ^3He above the regional value for the same depth or at sill depth for maxima within enclosed basins. The regional values were taken from a profile collected at 22°S along the arc front but away from volcanic centers (see Figures 2 and 12).
[d] Fe/Mn is the molar ratio of total dissolvable Fe to total dissolvable Mn and is expressed as a mean (±1 s.d.) rather than maxima.
[e] The "nd" notation signifies that a sample was acquired but a property value was not determinable.
[f] The dash ("–") symbol denotes that a sample was not collected.

surround a caldera measuring 8 by 5.5 km (Figure 11). Within the caldera are a series of large (up to 3 km in diameter) and deep (to 450 m) craters. A moderately intense, multilayered particle plume was present within the largest crater, but no Eh or pH anomalies were detected. Moderate-to-weak signals for the other chemical plume tracers were observed (Figures 6 and 7 and Table 1).

4.1.6. Volcano 18S

[20] This unusual volcano is dominated by a large funnel-shaped caldera ~6.5 km in diameter and >1100 m deep. A satellite cone rises to 270 mbsl from the eastern flank of the volcano (Figure 12). Two particle plumes were detected along a single towpath crossing the edifice: one filled the caldera below ~850 m depth, while a second, thinner but more intense, plume was mapped near the crest of the eastern satellite cone (Figure 12 and Table 1). A small negative deflection in the Eh profile was associated with the plume at the eastern cone, and an even lower voltage anomaly was present throughout the caldera. The shallow plume at this site had the second highest δ^3He anomaly, ΔpH, and Fe values and the highest average Fe/Mn (18.8) observed along the south Tonga arc (Table 1). The caldera was well-mixed with enrichments in ^{3}He, CH_4, and Fe comparable to the levels found in the shallow plume, while TDMn and PMn were slightly enriched (Figures 6 and 7 and Table 1). The concentrations of Fe and Mn peaked near sill depth.

4.1.7. Volcano 19

[21] A poorly preserved caldera, 3.5 by 2.5 km, forms the summit of Volcano 19. Within this is a large central cone complex rising to 385 mbsl, and to the west a younger western caldera 1.9 km in diameter (Figure 13). As at Volcano 18S, separate particle plumes were found within the western caldera and at the summit. In this instance, the more intense particle plume was found within the caldera (Table 1). The shallow summit plume is dispersed horizontally as a relatively low-intensity, 30-m-thick particle lens throughout the tow area and also was observed at a "background" station

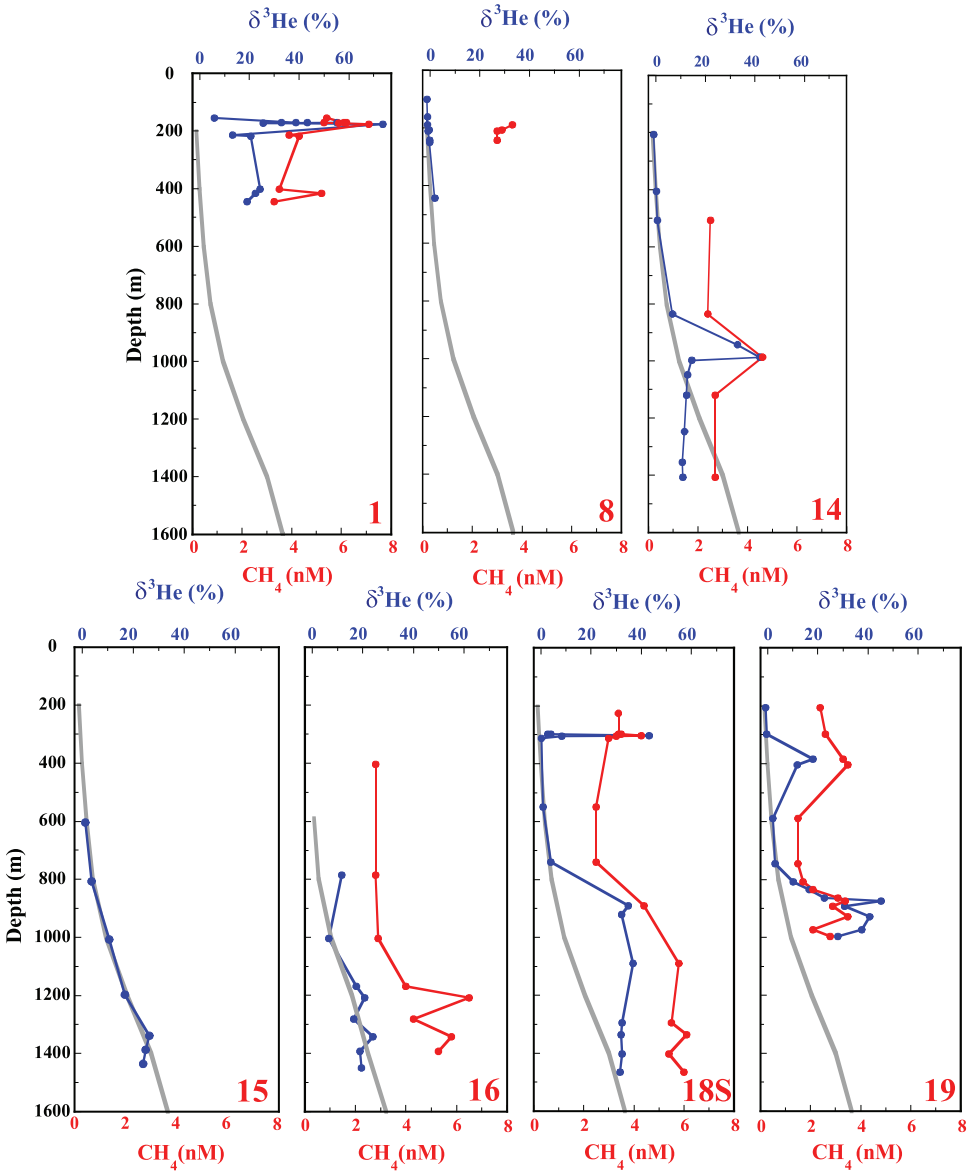

Figure 6. Discrete water sample results for δ^3He (%, blue data points and lines) and CH_4 (nM, red data points and lines) from tow-yo deployments at south Tonga arc volcanic centers with hydrothermal plumes. Designations of the volcanic centers are given in the bottom right-hand corner of each panel. The gray line repeated in each panel is the δ^3He profile for a sampling station located along the arc front at 22°S (orange star on Figure 2). This site is the farthest distant from an active volcanic center and is taken as representative of the regional depth distribution for δ^3He.

7 km to the south (Figure 2). A spike in Eh sensor voltage occurred within the deep central area of the western caldera. The shallow plume had weak to moderate levels for most of the chemical properties except for pH, for which no anomaly was detected (Table 1 and Figures 6 and 7). The caldera plume contained the highest concentrations of Fe and Mn measured along the south Tonga arc, δ^3He values that were substantially elevated above those for the shallow plume at this site, and a moderate pH anomaly.

4.2. Valu Fa Ridge Back Arc, Eastern Lau Spreading Center

[22] Our survey of back-arc plumes included 132 km of tows along and across the southern section of the VFR and vertical casts over the Hine Hina and Vai Lili vent sites and within the Mariner and Misiteli plumes (Figure 3). In order to compare the Valu Fa Ridge results with the physical properties of plumes on the adjacent south Tonga arc, we have reproduced the contour maps for ΔNTU and $\Delta\theta$

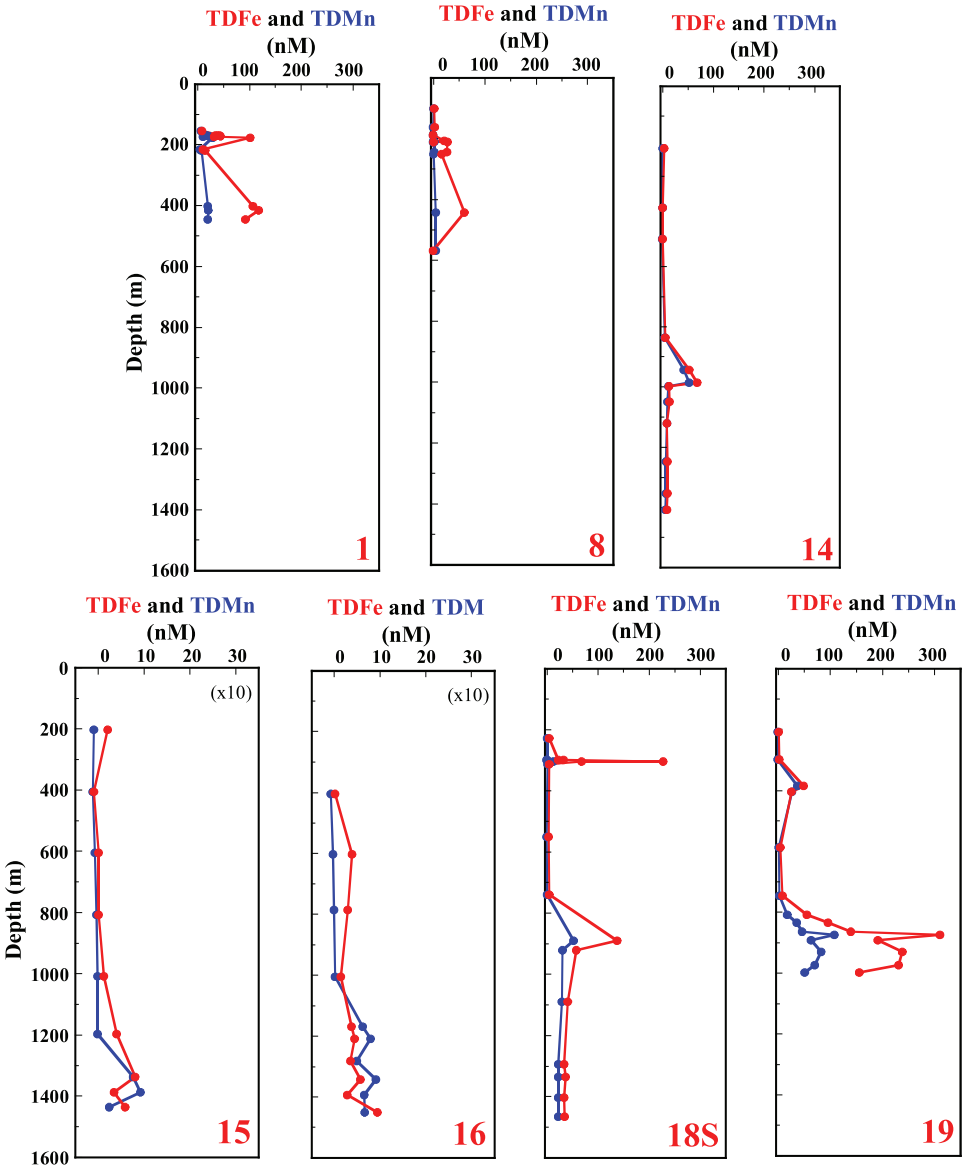

Figure 7. Total dissolvable iron (TDFe, nM, red data points and lines) and manganese (TDMn, nM, blue data points and lines) plume distributions at venting volcanic centers on south Tonga arc. The concentration scales for Volcanoes 15 and 16 are expanded by an order of magnitude relative to other sites.

and latitudinal profiles of Eh along the VFR, from which at least eight plumes were previously identified by *Baker et al.* [2005] (Figure 14). Here we present new data for five sites sampled for chemistry: the historical Hine Hina and Vai Lili vent sites (Figure 14, site numbers 1 and 8), which had either undetectable or weak physical property plumes, and plumes over the Misiteli, Mariner, and TELVE sites discovered during *TELVE* based on their more striking physical characteristics (Figure 14, site numbers 4, 9, and 11, respectively; Table 1).

4.2.1. Hine Hina

[23] Although diffuse seafloor venting was observed at the Hine Hina site shortly before and after our plume survey [*Fretzdorff et al.*, 2006; *Ishibashi et al.*, 2006], we were unable to distinguish a plume over this site using either physical (ΔNTU, $\Delta\theta$, and ΔEh) or chemical (ΔpH, ^{3}He, CH_4, Fe, and Mn) measurements (Table 1 and Figure 15). Instead, our observations seem to indicate a basin-wide accumulation of the more conservative plume tracers (such as δ^3He, TDFe and TDMn).

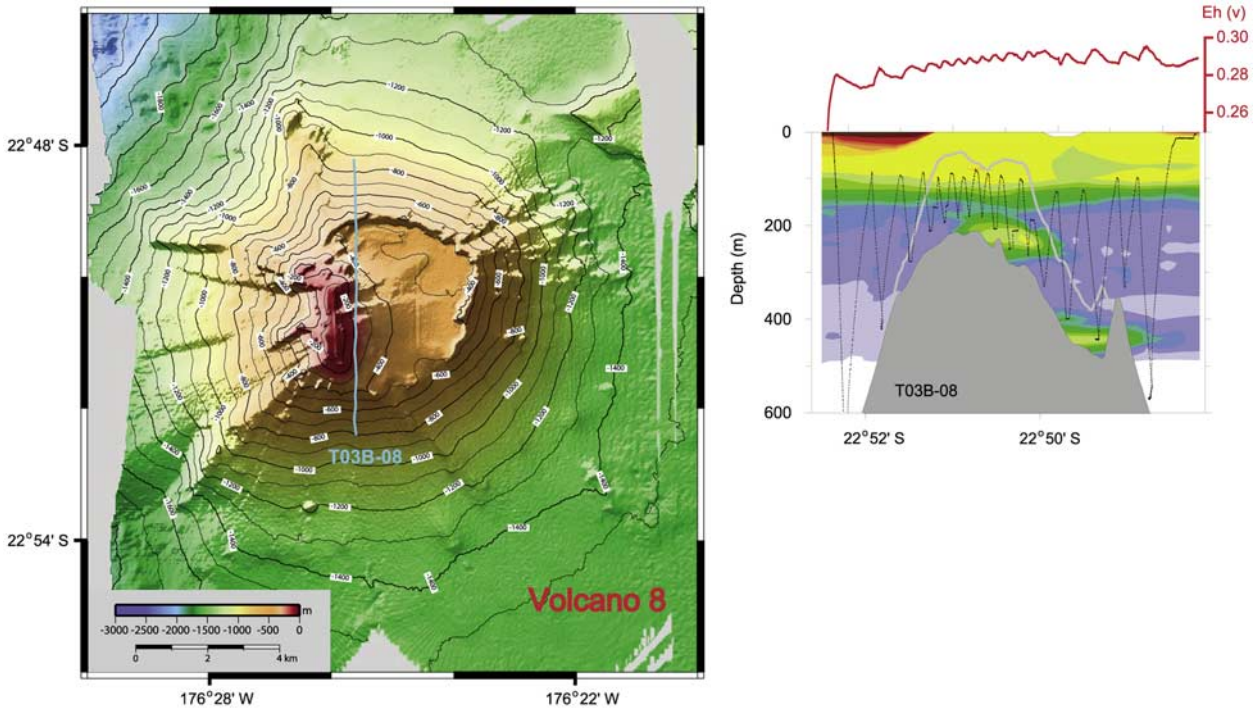

Figure 8. Towpath and plume distributions at Volcano 8 (Pelorus Reef). Raised bathymetry profile is along the summit ridge west of towpath. See Figure 5 caption for details.

4.2.2. Vai Lili

[24] We found generally weak physical and chemical plumes at this site (Table 1 and Figure 15), consistent with direct seafloor observations that this once high-temperature (340°C) vent field had been covered by lava prior to our *TELVE* survey [*Fretzdorff et al.*, 2006] and ~1.5 a after *TELVE* was discharging only warm spring fluids at a maximum temperature of 88°C [*Ishibashi et al.*, 2006]. In addition, the close proximity of the Vai Lili and Mariner vent fields make it difficult to distinguish their respective plumes. Although a minor thermal plume was located above the Vai Lili site (Figure 14), the origin of small particle and chemical anomalies throughout this region is less obvious.

4.2.3. Misiteli

[25] Located along the deep, northern tip of the Southern segment, and between the Hine Hina and Vai Lili sites, this plume was spatially impressive (it extended ~5 km along axis) but generally had weaker chemical anomalies compared to most plumes on this back arc and the adjacent arc (Table 1 and Figures 6, 7, and 15). The concentrations of PS and PMn within the Misiteli plume were comparable to sites along the south Tonga arc.

4.2.4. Mariner

[26] The Mariner plume was the largest and most intense (relative to the anomalies for all measured physical and chemical properties) of the VFR plumes (Table 1 and Figures 14 and 15). The plume extended >8 km along and 4 km across the strike of the Central segment. Compared to plumes on the south Tonga arc, the Mariner plume had a larger anomaly in Eh (−0.07 V), and ~2-times or higher concentrations of Fe and Mn (812 and 197 nM, respectively; Table 1). In contrast, anomalies indicative of volatile discharge (^{3}He, pH as proxy for CO_2 and sulfur gases, and CH_4) were small compared to maxima observed at several sites on the south Tonga arc (Table 1). The high concentration of PS (Table 1) is consistent with rapid oxidation-precipitation of H_2S gas measured in vent fluids at this site (~14 mM [*Ishibashi et al.*, 2006]).

4.2.5. TELVE

[27] Although the TELVE and Mariner plumes overlap slightly horizontally, they are separated

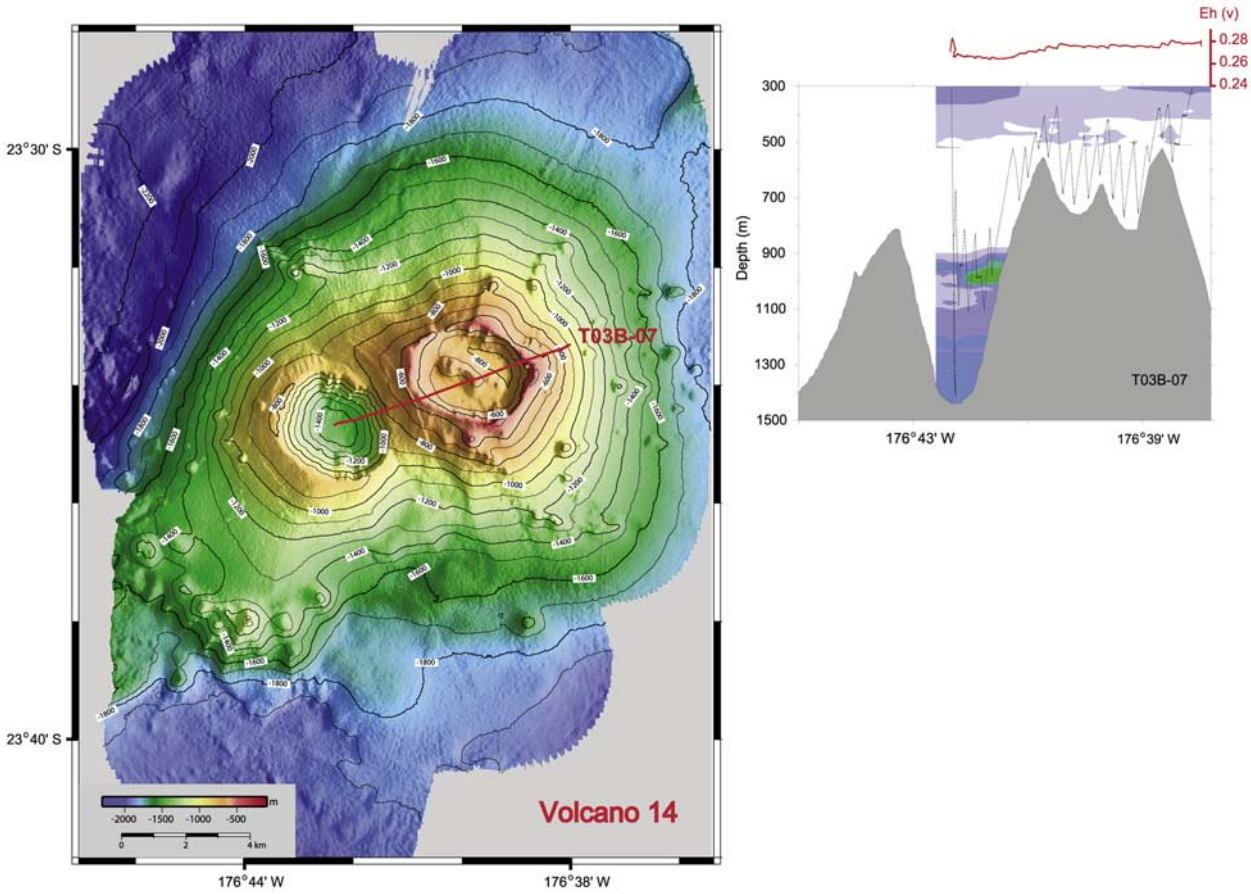

Figure 9. Towpath and plume distribution at Volcano 14. See Figure 5 caption for details.

vertically (Figures 2 and 14). Plume anomalies at the TELVE site were generally lower in magnitude compared to those arising from the Mariner field on the back arc.

5. Discussion

5.1. Spatial Distribution of Venting Along the Arc

[28] With the addition of our *TELVE* results, 50% of the Tonga-Kermadec arc has been surveyed for hydrothermal venting. The 425-km length of the south Tonga arc is twice the minimum survey length preferred for assessment of F_s, which is the venting site frequency expressed as sites/100 km of ridge length [*Baker and German*, 2004]. The F_s value for the south Tonga arc is 2.6 (11 sites/425 km of arc front), almost identical to the value of 2.5 obtained if we incorporate it with our earlier results from the southern and mid-Kermadec arc sections (total then ~32 sites/1265 km of arc front, where each site is listed as a separate plume/depth in summary tables here and by *de Ronde et al.* [2001, 2007]). This site density is comparable to the F_s value of 3.2 for the MOR systems in the eastern Pacific (73 sites/2280 km [*Baker and German*, 2004]).

[29] The 190-km-long gap in venting that occurs between Volcanoes 1 and 8, where 5 vent sites would be predicted using the segment F_s value, is highly anomalous and associated with an unusual number of major, active and degraded, volcanic constructs (Figure 2) (T. Worthington et al., manuscript in preparation, 2007). Perhaps not coincidentally, the VFR is only 30–60 km west of this arc segment. The unusual hybrid arc-MOR geochemistry of the VFR lavas requires the involvement of a component derived from the subducting slab, either directly or by capture of magma from the adjacent arc [*Martinez and Taylor*, 2002, 2003; *Taylor and Martinez*, 2003; *Martinez et al.*, 2006]. Thus we consider that the actively spreading VFR may have captured some proportion of the magma ascending beneath the adjacent south Tonga arc. Taking the full latitudinal extent of the magmatically inflated VFR between 21°26′ and 22°44′S

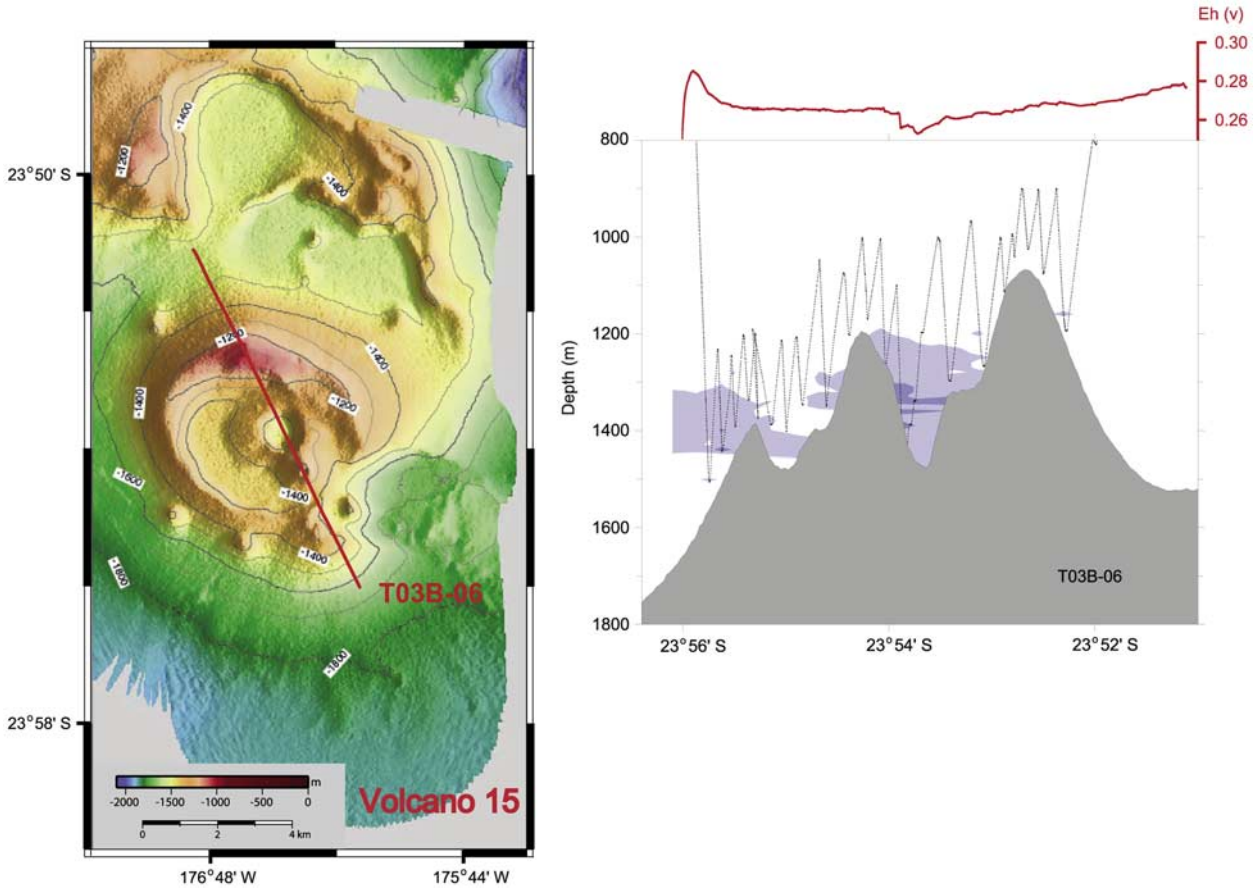

Figure 10. Towpath and plume distribution at Volcano 15. See Figure 5 caption for details.

(152 km, the true length is underestimated by the extent of ridge crest overlap), and counting the number of discrete plumes mapped there as 10 [*Martinez et al.*, 2006; *Baker et al.*, 2006], the vent field density is 6.6 sites/100 km. This is three-times that expected from either a similar spreading MOR [*Baker and German*, 2004] or that seen elsewhere along the surveyed sections of the Tonga-Kermadec arc [*de Ronde et al.*, 2001, 2007; *Baker et al.*, 2003], which we consider a remarkable coincidence. Therefore we suggest that the unusually high field density on this part of the VFR represents the "missing" vent fields of the south Tonga arc together with a "normal" MOR-like component. A similar interpretation may be appropriate for the vent field density along the north Tonga arc, where capture of magmas by the nearby Fonualei Spreading Center may occur (Figure 1).

5.2. Chemical Implications of Venting Near the Convergent Plate Edge

[30] In this section we address the chemical nature of the plumes sampled on the south Tonga arc and Valu Fa back arc: how they compare to one another in composition, intensity and variability, and to other plumes on this arc system and at MORs in the eastern Pacific. We further question whether these plumes might contribute significantly to both local and wider Pacific basin hydrothermal inventories. We frame our comments according to three types of plume tracers: ^{3}He, an unequivocal indicator of hydrothermal discharge; reactive magmatic gases (e.g., CO_2, SO_2, and H_2S) that are often characteristically enriched in arc fluids; and Fe and Mn, commonly present as major ionic components in vent fluids.

5.2.1. He-3

[31] Because ^{3}He commonly enters the oceans only via hydrothermal pathways and is both inert and highly resolvable analytically, it serves as an unequivocal and primary tracer of submarine venting regardless of tectonic setting (e.g., at MORs, intraplate volcanoes, arcs, and back-arc ridges). The origin of vented ^{3}He, however, can be complex and intimated using R/Ra values. *Hilton et al.* [2002]

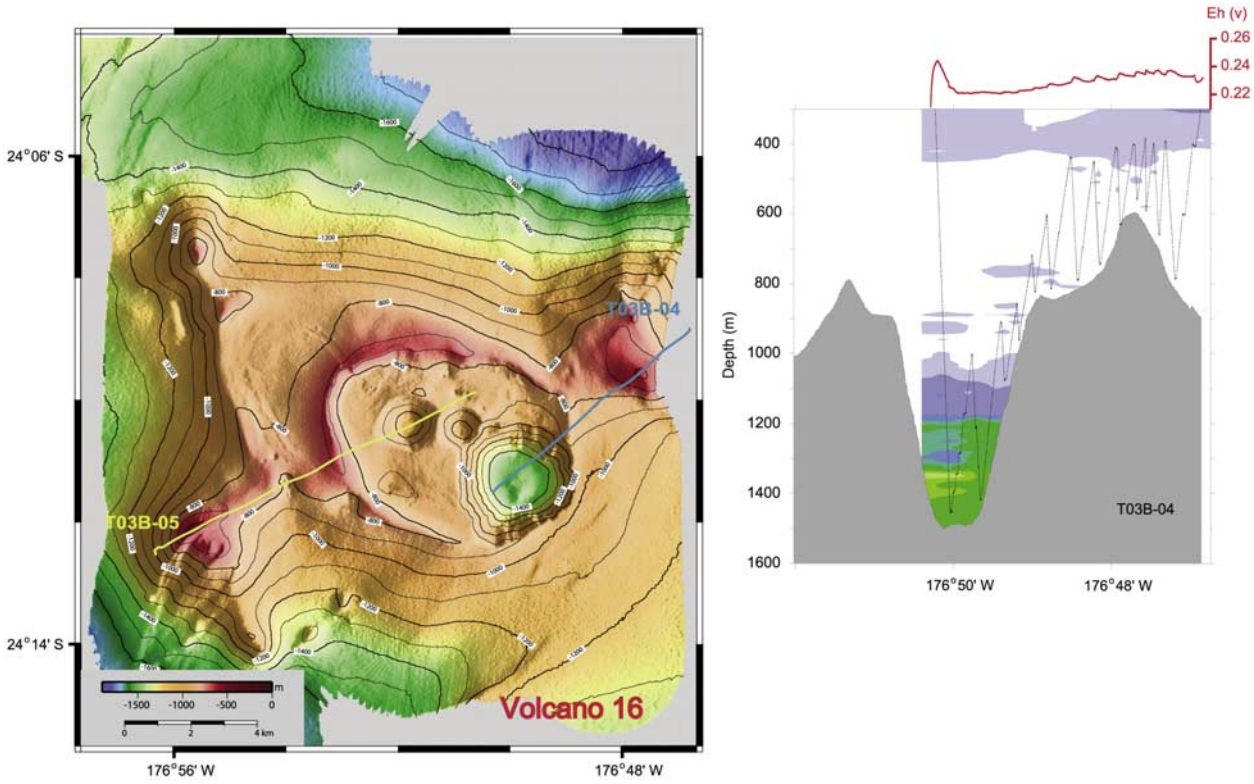

Figure 11. Towpath and plume distribution at Volcano 16. See Figure 5 caption for details.

reviewed global data from 26 subaerial arc segments and calculated a mean R/Ra of 5.4 ± 1.9, effectively below the canonical MORB-He isotope range of 8 ± 1, which reflects an upper mantle source. They interpreted ^{3}He in arc samples with R/Ra <7 also to be predominantly of mantle origin, but diluted slightly with (radiogenic, R/Ra = 0.02) ^{3}He from arc crust and/or lithosphere that magmas must transit before reaching the seafloor. Our data for the south Tonga arc are similarly "arc-like": helium isotope results for samples from the summit plume at Volcano 1 have an R/Ra value of 6.9 ± 1.4. Unfortunately this is the only site within our arc/back-arc survey where ^{3}He was sufficiently abundant (δ^3He anomaly values >30% are required for confident prediction of vent fluid attributes using plume data) or where there were enough data points to determine an R value by regression analysis. While limited, our data for the southern Tonga arc are consistent with those for plumes along the Kermadec arc, where the range in R/Ra was 5.9–7.4 [*de Ronde et al.*, 2001, 2005, 2007; *Massoth et al.*, 2003].

[32] Regional data for δ^3He collected along the Tonga-Kermadec arc front suggest ^{3}He may be accumulating within the southern Lau Basin between 500 and 2000 m depth (Figure 16a; we note that the Lau Basin area surveyed during *TELVE* is separated from the eastern Pacific below ~500 m depth by the Tonga Ridge [*Wright et al.*, 2000]). Because this accumulation is greatest below about 1700 m depth, venting from the VFR is its most logical source (Figure 16b and Table 1; note that the arc profiles have been truncated at sill depth and that a single, representative vertical profile above the Mariner vent field is shown for the back arc where elevated concentrations extended to ~2000-m depth). We reject other plumes known within the Lau Basin as being the source of the local accumulation, either because they are too deep (e.g., multiple plumes along the ELSC north of 21°26′S [*Martinez et al.*, 2006; *Baker et al.*, 2006]), or too distant (the Tonga-Fiji plume, which was sampled ~880 km NNE of the *TELVE* area [*Lupton et al.*, 2004]). Although contributions of ^{3}He above 500 m depth are not apparent in the regional profiles (other than at the southernmost Tonga arc station, see caption for Figure 16), this does not necessarily indicate that the hydrothermal flux from the arc is insignificant. Shallow hydrothermal discharge from the various arc sites is typically more widely distributed in depth than discharge along ridgecrests, which can be concen-

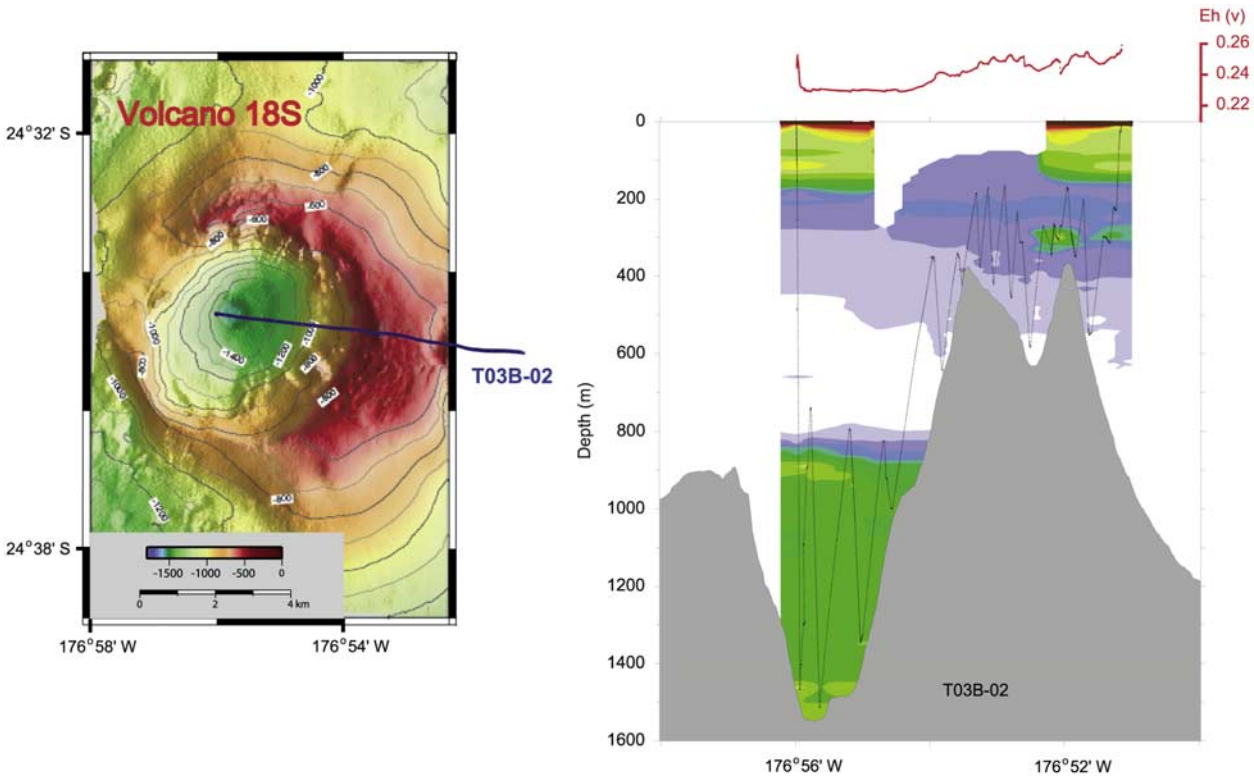

Figure 12. Towpath and plume distributions at Volcano 18S. See Figure 5 caption for details. Note that a narrow spike of high ΔNTU values within the summit plume has been muted by grid averaging.

trated by along-axis flow. In addition, helium injected at shallow depths may be more vulnerable to loss by exchange with the atmosphere and to dilution by turbulent mixing and advection.

[33] The magnitude of the δ^3He anomalies on the south Tonga arc were generally larger than on the VFR, where the largest anomaly of 20% δ^3He (Mariner plume) was exceeded at 6 of the 11 arc sites (Table 1). Anomaly magnitudes of >20% in δ^3He were also measured at 7 of 10 and 4 of 11 sites on the southern and mid-Kermadec arc [*de Ronde et al.*, 2001, 2007]. Plumes on MORs in the eastern Pacific similarly have anomalies that often exceed 20% (although we note that the δ^3He anomaly at the highly referenced 21°N EPR site is only 12% [*Lupton et al.*, 1980]), and occasionally exceed three or more times that value [e.g., *Lupton*, 1990; *Lupton et al.*, 1993; *Massoth et al.*, 1994; *Embley et al.*, 1998] as they also do on the Kermadec arc [*de Ronde et al.*, 2003, 2005, 2007]. It is our general impression that the magnitudes of plume enrichments in ^{3}He are comparable on both the divergent and convergent margins of the Pacific plate.

5.2.2. Reactive Magmatic Gases (CO_2, SO_2, and H_2S)

[34] Multiple sites marked by the copious discharge of magmatic (acid) volatiles (primarily CO_2-SO_2-H_2S in variable mix) have been identified on each of the surveyed arc fronts (e.g., the southern Kermadec [*de Ronde et al.*, 2001; *Massoth et al.*, 2003], mid-Kermadec [*de Ronde et al.*, 2007] and Mariana [*Resing et al.*, 2003; *Embley et al.*, 2004, 2006; *Lupton et al.*, 2006]). While this style of discharge is not unique to arcs (e.g., it occurs as pulsed magmatic events at MORs and at degassing intraplate volcanoes), our growing observations suggest it may be most common in this tectonic setting (or wherever venting from volatile-rich arc-like lavas occurs). Plume anomalies in pH provide a sensitive but non-discriminating indicator of this magmatic discharge (i.e., each of the primary magmatic gases can produce acid when mixed with seawater [*Resing et al.*, 2004]). We consider pH anomalies to be "excessive" if they are larger than −0.04 pH, the upper limit for chronic plumes reported on MORs [*Baker et al.*, 2002; *Resing et al.*, 2004]. On the south Tonga arc, 3 of 11 vent sites had excessive pH anomalies (Table 1), which

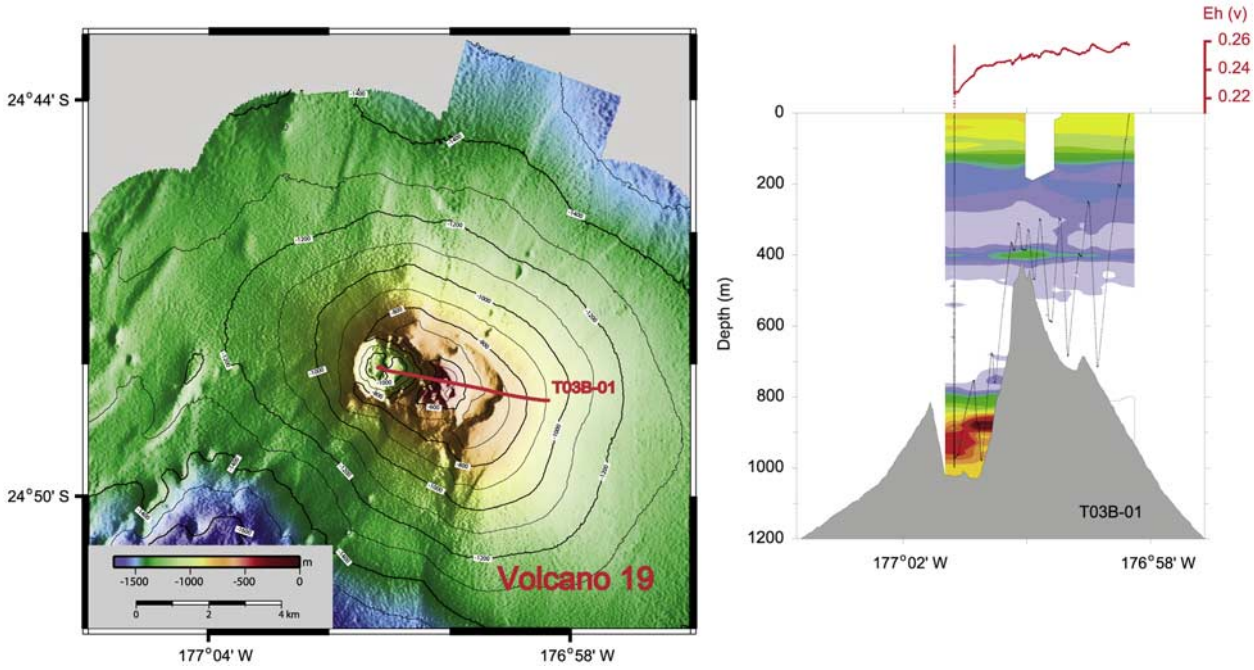

Figure 13. Towpath and plume distributions at Volcano 19. See Figure 5 caption for details.

compares to 6 of 10 and 4 of 11 sites on the southern and mid-Kermadec arc sections [*de Ronde et al.*, 2001, 2007; *Massoth et al.*, 2003]. However, the very large anomalies measured on the Kermadec arc (four sites ranged between −0.22 and −0.39 ΔpH) were not matched on the south Tonga arc, where the largest value was −0.08 ΔpH (in the summit plume at Volcano 1, where *Stoffers et al.* [2006] reported a total gas concentration of 130 mM in vent fluids). In contrast, on the VFR, pH anomalies were everywhere MOR-like, which is surprising given the significant influence of magmatic volatiles on vent fluids at the Mariner site (e.g., the total gas concentration was ∼80 mM and the pH 2.4 [*Ishibashi et al.*, 2006]), and the preponderance of arc-like lavas there (Table 1).

[35] Although dissolved H_2S has been measured directly in 8 different plumes on the southern Kermadec and Mariana arcs [*de Ronde et al.*, 2001; *Massoth et al.*, 2003; *Resing et al.*, 2003], we failed to detect this gas at any of the *TELVE* survey sites. Consistent with this, the concentrations of particulate sulfur (PS) determined in the south Tonga arc plumes were low (≤21 nM; Table 1) relative to levels observed on other arc segments (10^2–10^3 nM [*Massoth et al.*, 2003; *Resing et al.*, 2003; *de Ronde et al.*, 2007]). Together, the results for pH and sulfur suggest that while fluids enriched in magmatic volatiles are discharging on the south Tonga arc (and VFR), the intensity and instance of this discharge is generally less than on other surveyed arcs.

5.2.3. Fe and Mn

[36] Because they are commonly major aqueous ionic components of submarine vent fluids (as reviewed by *Hannington et al.* [2005]), and have a long residence time in the water column making them resolvable analytically even as distant plumes [e.g., *Klinkhammer and Bender*, 1980; *Boyle et al.*, 2005], Fe and Mn are useful tracers of seafloor venting. Enrichments in Fe were detected within all of the identified arc plumes (Table 1), although at Volcanoes 15 and 16 the Fe excess was marginal (∼3× that at non-plume depths) and not perfectly aligned with other plume tracers, possibly reflecting sediment re-suspension. Coincident Mn plumes occurred everywhere on the arc except at Volcano 8. The relatively high concentrations of particulate Mn (∼5 nM) observed within the calderas of Volcanoes 1, 18S, and 19 (Table 1) likely reflect progressed "aging" of the plumes trapped within these basins [e.g., *Cowen et al.*, 1990]. On the VFR, plume concentrations of Fe and Mn were most pronounced at the Mariner, TELVE, and Vai Lili sites: Mariner had the highest concentration of TDFe observed during the *TELVE* survey (812 nM), and the concentrations of TDMn at all three sites exceeded those on the South Tonga arc (Table 1). Generally, high ambient concentrations of Fe and

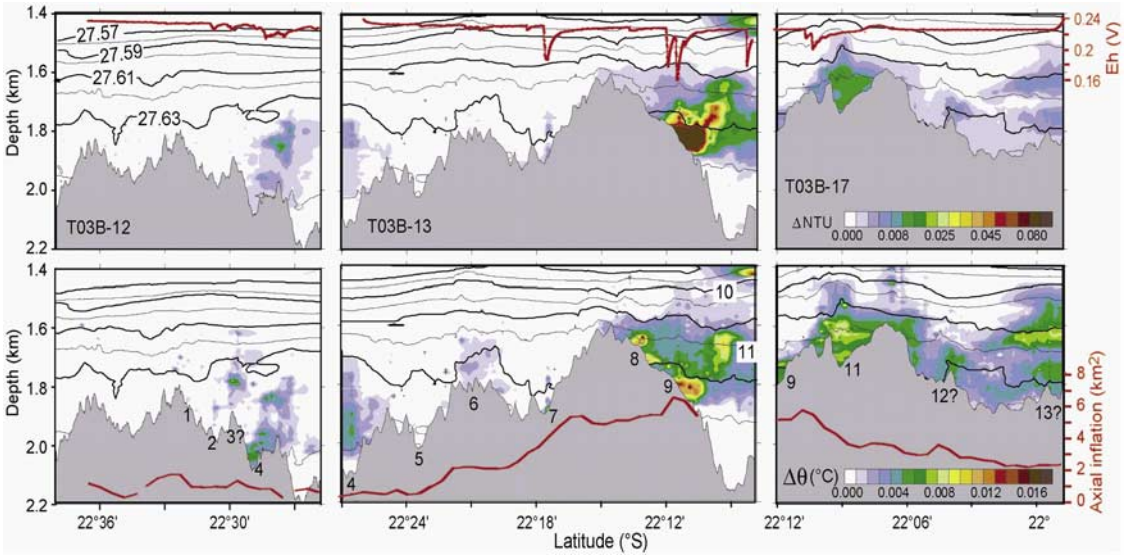

Figure 14. Transects of plume anomalies along the southern VFR. (top) Contoured ΔNTU anomalies for along-axis tows (except T03B-11, where no anomalies were detected). Color scale is identical to that used for south Tonga arc contour maps (Figures 5 and 8–13). Corresponding Eh profiles are shown as red lines embedded along the top panels; scale in relative volts is on right axis. (bottom) Contoured $\Delta\theta$ values. Red lines at the bottom of panels indicate cross-axial inflation (scale on right axis of the T03B-17 panel) from *Martinez and Taylor* [2002]. Numbers along the bathymetry underlie individual plumes; 3, 12, and 13 may not have underlying sources. Plumes 1 (no anomalies) and 8 correspond to the Hine Hina and Vai Lili vent fields, and 4, 9, and 11 correspond to the Misiteli, Mariner, and TELVE vent sites, respectively. For all panels the bathymetry corresponds to the tow track, and the black contours are for potential density, σ_σ, labeled in the T03B-12 ΔNTU panel. From *Baker et al.* [2005], reproduced with permission.

Mn occurred at plume depths along the VFR south of the Mistelili site (e.g., the concentrations reported for Hine Hina, Table 1), and also below 1600 m depth at "background" stations located along the arc front (Figure 2), where the mean concentrations of TDFe and TDMn exceeded those at shallower depths by ~4 and 7 nM, respectively (not shown). We interpret these observations, like those above for δ^3He, as indicative of an accumulation of hydrothermal effluent within the southern Lau Basin.

[37] Variations in Fe-to-Mn values can be used to help differentiate the sources of these metals and also to provide clues regarding subseafloor processes responsible for their relative abundances [e.g., *Bostrom and Peterson*, 1966; *Massoth et al.*, 2003; *Malahoff et al.*, 2006]. For the south Tonga arc, a large range in Fe/Mn values (0.8 to 18.8) was observed (Figure 17 and Table 1), similar to the ranges reported for the southern and mid-Kermadec arc sections (0.2–18 and 0.5–9, respectively [*Massoth et al.*, 2003; *de Ronde et al.*, 2007]). The relatively high Fe/Mn values at Volcanoes 1 (caldera), 8, and 18S (E. cone) suggest fluids enriched in magmatic volatiles may be discharging from these sites [*Massoth et al.*, 2003; *de Ronde et al.*, 2007], which is consistent with the pH values at these sites. The Fe/Mn values at other arc sites were considerably lower (range of mean values: 0.8–3) and similar to those on the VFR (range of means: 0.9 and 2; Figure 17 and Table 1). Not coincidently, these ranges closely match that for the hydrothermal component of sediments previously recovered from the flanks of the VFR (1.2–2.8) [*Daesslé et al.*, 2000], which have some of the highest concentrations of Fe and Mn reported near any spreading ridge [*Cronan and Hodkinson*, 1997]. *Cronan and Hodkinson* [1997] attributed these high concentrations to fallout of hydrothermal Fe and Mn trapped within the semi-enclosed Lau Basin, consistent with our findings of hydrothermal accumulations in the deep water column throughout the *TELVE* study area.

[38] The high ratios of Fe/heat and Mn/heat for the VFR, and the Mariner site in particular, suggest Fe and Mn are being hydrothermally mined there at high efficiency relative to MORs in the eastern Pacific (Table 2). Given the similar co-variances in plume incidence with spreading rate for VFR and MOR spreading segments [*Baker et al.*, 2006], this

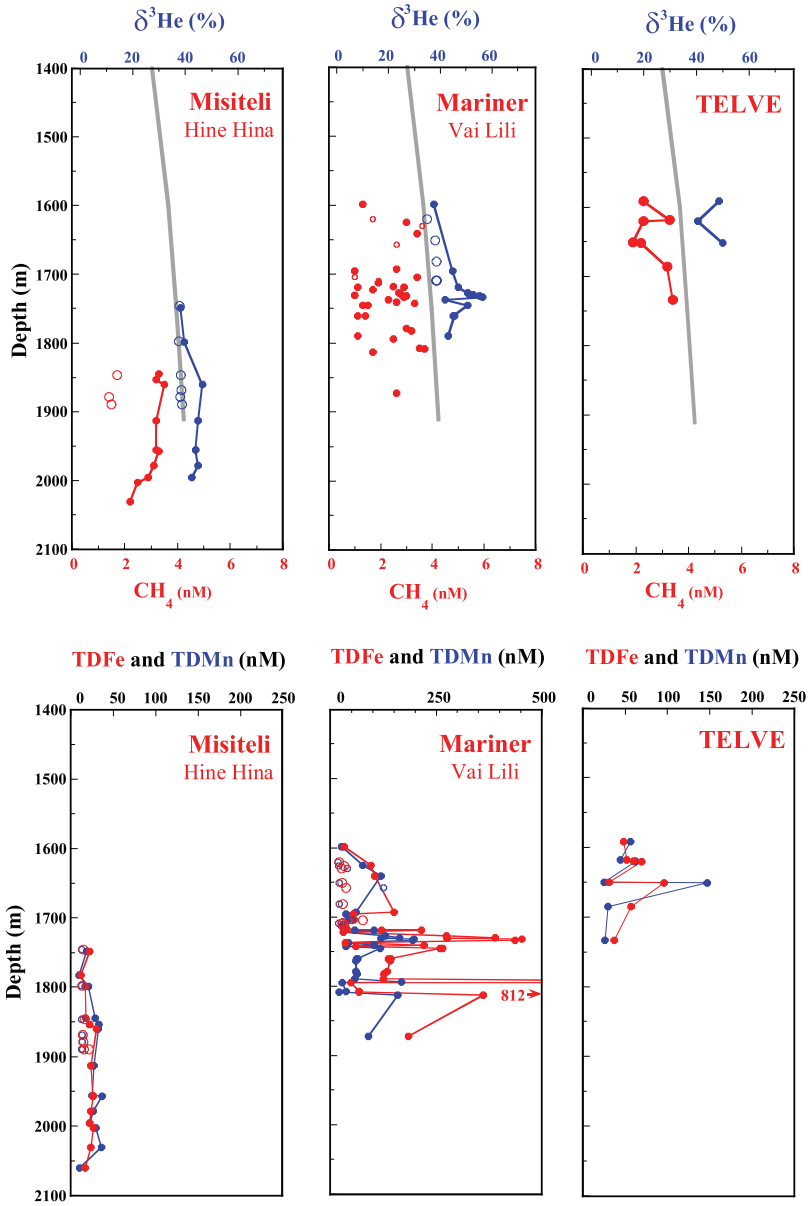

Figure 15. Chemical data for plumes along the Southern (Hine Hina and Misiteli sites, left-hand panels), Central (Vai Lili and Mariner sites, middle panels), and Northern (TELVE site, right-hand panels) segments of the VFR. Open symbols denote data from the Hine Hina and Vai Lili sites. (top) Data for δ^3He (%) are shown as blue data points and lines, and data for CH_4 (nM) are shown as red data points and lines. The gray line repeated in each top panel is the regional δ^3He profile, as in Figure 12. (bottom) Data for total dissolvable iron (TDFe, nM) are shown in red, and data for total dissolvable Mn (TDMn, nM) are shown in blue.

higher extraction efficiency may translate into large fluxes that contribute to the observed accumulations of these metals in the water column and sediments. We cannot ascribe the higher metal/heat values to the compositions of the arc-like lavas on the VFR (Table 1), as the groundmass abundances of Fe and Mn are typically lower than for basalts on MORs [*Stanton*, 1994]. More logically, the metal enrichments are due to the presence of a magmatic (acid) volatile component within the VFR fluids, as described by *Ishibashi et al.* [2006]. Comparing the maximum value for Fe concentration with the corresponding fluid temperature at the Mariner site (~12.5 mM and 365°C) yields a Fe/heat value of ~4.5 nM/J, similar to that found in the overlying plume (Table 2).

[39] To compare the concentrations of Fe and Mn in plumes on the south Tonga arc and Valu Fa back arc to one another and to plumes elsewhere along

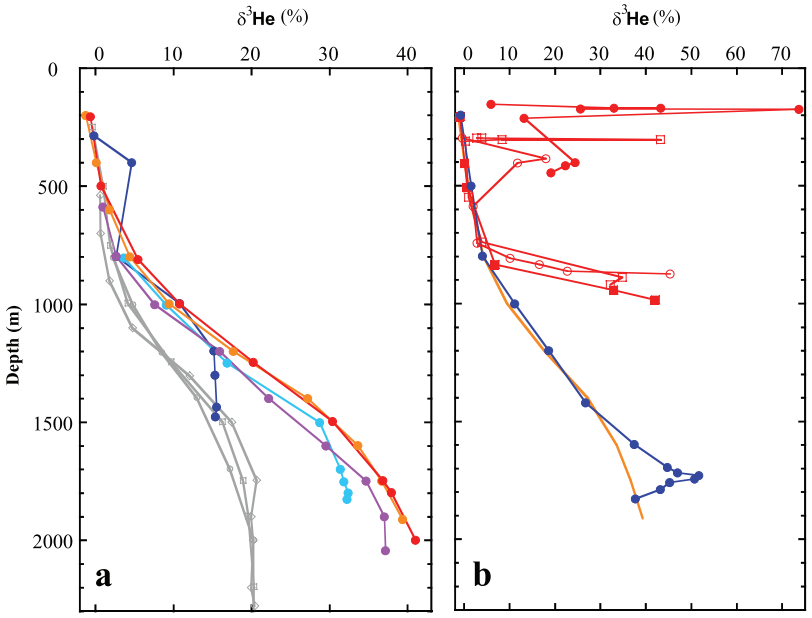

Figure 16. Depth profiles for δ^3He (%). (a) Selected regional profiles along the Tonga-Kermadec arc; all stations are located away from major volcanic centers. The profiles in gray demonstrate the similar depth distribution of δ^3He along a 910-km-long section of the Kermadec arc (station locations are at 35.3°S, 33.1°S, and 27.6°S; concentrations at ~1700 m depth increase slightly south to north). The colored profiles represent the south Tonga arc (color-keyed to station location stars on Figure 2), where the southernmost station (dark blue) is located ~320 km north of the gray grouping. Deeper concentrations generally increase south to north. The 385-m-depth plume at Volcano 19 clearly influences at the southernmost profile (dark blue), collected only 7 km south of that volcanic center. (b) Profiles for arc (in red: Vol. 1, closed circle; Vol. 14, closed square; Vol. 18S, open square; Vol. 19, open circle) and back-arc (in blue: only a single profile at Mariner site is shown) plumes where δ^3He values exceed the regional concentration by ~20% (Table 1). Note that arc profiles are truncated at the respective sill depths. The regional profile (orange line) is repeated from Figure 16a. Figure 16b illustrates the ~600-m depth separation between plumes dispersing from the south Tonga arc and adjacent Valu Fa back arc.

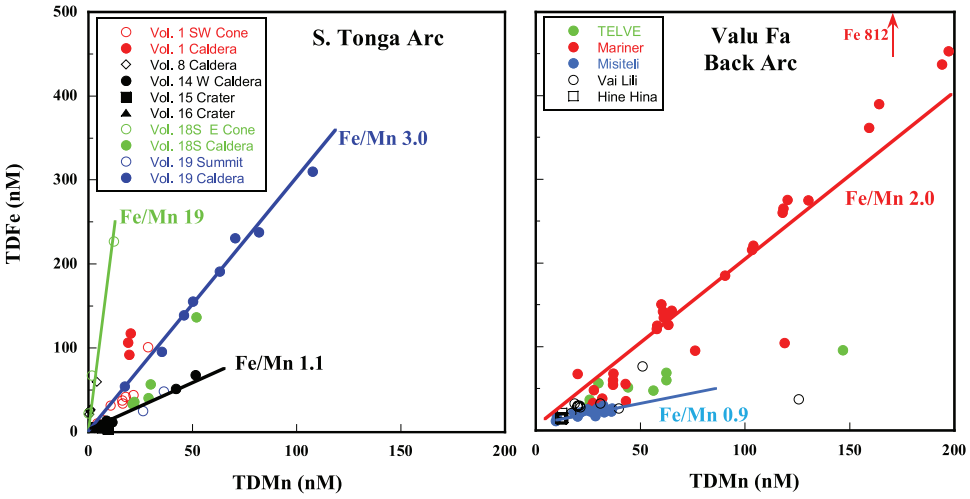

Figure 17. Iron (TDFe, nM) versus manganese (TDMn, nM) relations for (left) the south Tonga arc and (right) Valu Fa back arc. Line and slope values represent means for the respective data groups, which are color-coded to the panel keys and listed in Table 1.

Table 2. Fe/Heat and Mn/Heat Values for VFR and Other Plumes

Site	N[a]	Fe/Heat,[b] nmol/J	Mn/Heat, nmol/J
TELVE	4	1.6 ± 0.5	1.9 ± 1.1
Mariner	17	5.2 ± 2.7	2.3 ± 0.8
Vai Lili	4	1.0 ± 0.7	1.4 ± 0.9
Misiteli	12	0.6 ± 0.1	0.7 ± 0.1
Brothers NW[c]	7	2.5 ± 1.5	0.5 ± 0.2
EPAC MORs[d]	range of means	0.8 − 2.0	0.3 − 0.7

[a] N is number of data points used to determine mean ±1 std. dev.
[b] Heat capacity value for seawater of 3915 J kg^{-1} was used to assess ratio values. Thermal anomalies for the Valu Fa plumes ranged from 0.008° to 0.019°C (Figure 14).
[c] Brothers NW is a vent site within a closed caldera at Brothers volcano on the southern Kermadec arc [from *Massoth et al.*, 2003].
[d] EPAC MORs (East Pacific Mid-Ocean Ridges) include Juan de Fuca Ridge [*Massoth et al.*, 1994; 1995; *Resing et al.*, 1999], Gorda Ridge *Massoth et al.*, 1998], and Southern East Pacific Rise between 14°–18.5°S and 27°30′–32°18′S [*Massoth and Hey*, 1998]. Note that the range of mean values for the subsets is given in place of a composite mean and std. dev.

the Pacific plate edge, we have assembled the data in Table 3. Additionally, we present the (Fe + Mn) data from Table 3 graphically, where it is indexed to the plume depths for the surveyed regions on the plate margin (Figure 18). Even though there are large standard deviations associated with the mean value data (Table 3), we feel this approach more closely reflects the relative bulk abundances of Fe and Mn dispersed in these plumes than comparisons based on maximum values that rely on a single data point for each region. The south Tonga arc has the lowest average concentration of (Fe + Mn) of the three reported sections of the Tonga-Kermadec arc, each having plume depths that range between ∼100 and ∼1500 m. The average concentration of (Fe + Mn) on the VFR is slightly greater than that for the south Tonga arc, but less than the average values for the southern and mid-Kermadec arc sections. Plumes on the VFR are focused within a ∼220-m-thick layer centered at 1790 m depth. Plumes within the four sections of MOR surveyed in the eastern Pacific have average (Fe + Mn) concentrations that span the range of values for the arc and back arc. Plume depths for the MOR sections are consistently deeper than for the arc sections, and range between 2000 and 2600 m depth. The data shown in Figure 18 represent large segments of the convergent (1265 km of arc front) and divergent (1555 km of MOR) edges of the Pacific plate. The comparable concentrations and variability of the (Fe + Mn) plumes along these respective plate edges confirm our expectation based on a common hydrothermal genesis, and provide convincing support to the notion that arcs may be important to the overall hydrothermal input to the Pacific basin.

[40] We note that venting into the shallow waters of the Pacific is restricted, at least along the magmatic plate edges, to arc volcanoes. Along the half of the Tonga-Kermadec arc now reported,

Table 3. Average Fe and Mn Data for Plumes Along the Boundary of the Pacific Plate

Section[a]	Length, km	Depth,[b] m	N[c]	Fe,[d] nM	Mn,[d] nM	Fe + Mn, nM	Fe/Mn, mol/mol
			Frontal Arc				
S. Tonga	425	170–1340	32	91 ± 76	32 ± 23	122 ± 79	4.3 ± 7.9
Mid-Kermadec	580	120–1360	69	140 ± 422	41 ± 85	181 ± 430	4.6 ± 6.9
S. Kermadec	260	190–1455	231	193 ± 370	49 ± 76	242 ± 378	5.4 ± 5.5
			Back-Arc Ridge				
Valu Fa	88	1790 ± 109	72	98 ± 136	53 ± 48	151 ± 144	1.6 ± 0.7
			Mid-Ocean Ridge				
JdFR Cleft	55	2098 ± 119	305	164 ± 129	82 ± 56	246 ± 188	1.9 ± 0.7
NEPR 8–12N	350	2380 ± 224	58	36 ± 46	19 ± 14	55 ± 48	1.8 ± 2.7
SEPR 14–18S	540	2479 ± 69	99	213 ± 190	34 ± 21	247 ± 191	5.8 ± 3.5
SEPR 27–32S	610	2220 ± 132	256	129 ± 298	42 ± 67	171 ± 305	3.1 ± 1.5

[a] Entries have been restricted to data sets representing large sections of the plate boundary or, in the case of Cleft segment, a near-decadal time series. All data are believed to represent chronic hydrothermal discharge; all samples with metal concentrations >∼10 nM have been included. Data sources: south Tonga arc and Valu Fa back arc, this study; mid-Kermadec arc 29°–34.5°S, *de Ronde et al.* [2007]; southern Kermadec arc 34.5°–36.5°S, *de Ronde et al.* [2001, 2007] and *Massoth et al.* [2003]; Juan de Fuca Ridge, Cleft segment, *Massoth et al.* [1994]; NEPR, Northern East Pacific Rise 8.7°–11.8°N, *Feely et al.* [1994] and *Mottl et al.* [1995]; SEPR, Southern East Pacific Rise 13.8°–18.7°S and 27.5°–32.3°S, *Massoth and Hey* [1998].
[b] Range of depths of plume maxima along arc sections is given, whereas the mean of sample depths ±1 std. dev. is given for the ridge sections.
[c] N is the number of samples used to determine mean values.
[d] Total dissolvable Fe and Mn were determined everywhere except the NEPR, where particulate Fe and dissolved Mn were measured.

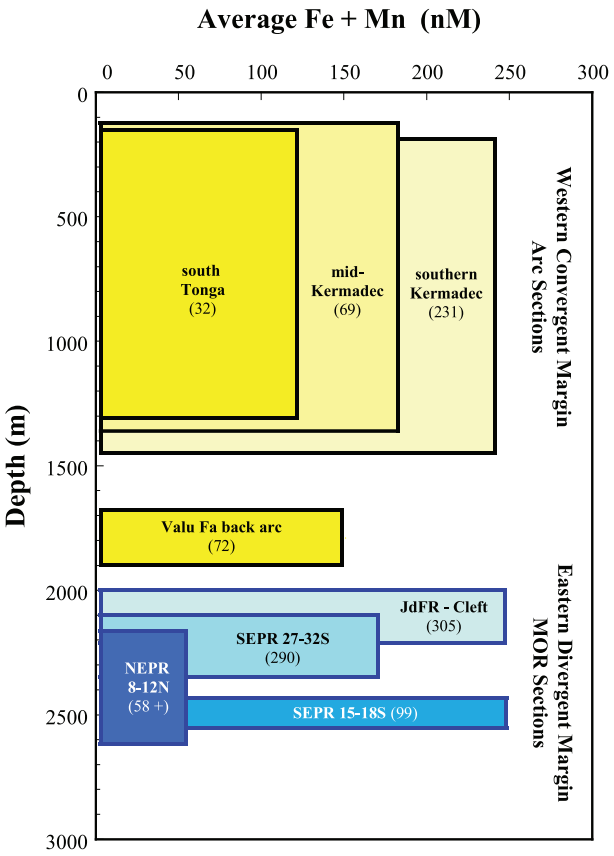

Figure 18. Average concentrations of (Fe + Mn) in hydrothermal plumes bounding the Pacific plate: the western, convergent plate margin is represented by sections of frontal arc surveyed between 1999 and 2004, and the eastern, divergent plate margin is represented by MOR sections surveyed during the preceding 13 a. Data and references are given in Table 3. Note that the plumes for the different tectonic settings occupy separate depth regimes that increasingly deepen in the following order: arc, back arc, MOR.

there are 11 plumes at depths of <500 m, many with concentrations of Fe that exceed several hundreds of nM (Table 1) [*de Ronde et al.*, 2001, 2007]. Most of this Fe exists as colloidal and particulate Fe(III) oxyhydroxides, following rapid oxidation of Fe(II) [*Field and Sherrell*, 2000] and precipitation/aggregation after discharge [*Massoth et al.*, 1998]. Even a very small fraction of this Fe may be sufficient to stimulate primary production in high nitrate, low chlorophyll (HNLC) regions of the ocean [e.g., *Coale et al.*, 1996; *Boyd et al.*, 2000]. Contributions of hydrothermal Fe to the equatorial Pacific Ocean, tentatively linked to sources located near the source waters of the Equatorial Undercurrent in the island arc region of Papua New Guinea, have been considered as an important driver of productivity [*Coale et al.*, 1996; *Wells et al.*, 1999]. We suggest that venting of Fe from shallow intraoceanic arc volcanoes, such as those on the Tonga-Kermadec arc, may similarly contribute to productivity within the Pacific basin.

[41] If we accept that venting site density and plume chemical intensity (for ^{3}He, Fe and Mn) are similar along the submarine western and eastern boundaries of the Pacific plate, where the ratio of intraoceanic arc front to MOR length is ~0.7 (intraoceanic arcs extend ~6380 km [*de Ronde et al.*, 2003]; MORs extend ~9000 km between 50°N and 37°S), then a significant contribution to the total hydrothermal inventory within the Pacific basin from arcs would be expected. While comparisons such as this provide important perspective regarding submarine fluid discharge from different volcanic and tectonic settings, we recognize that the spatial frequency of venting and fluid composition are only two measures that enter into the complex assessment of fluid flux, which is the most important point of comparison. Additional surveys, such as those embodied by *TELVE*, will help constrain the flux of hydrothermal fluids to the Pacific basin, particularly with respect to site density and fluid chemical character on convergent plate margins.

6. Summary

[42] 1. A systematic survey for hydrothermal plumes was completed along 425 km of the south Tonga arc (21°09′–24°48′S; 15 volcanic centers) and along 88 km of the back-arc VFR (21°58′–22°44′S). Eleven plumes were discovered on 7 south Tonga arc volcanic centers. Five of 8 sites mapped with underlying sources were sampled for chemistry along the VFR.

[43] 2. A vent field density of 2.6 sites/100 km of arc length was determined for the south Tonga arc, and a much higher density of 6.6 sites/100 km for the VFR. An anomalous ''plume-gap'' occurs along the south Tonga arc adjacent to the proximal VFR. We propose that the high field density of the VFR reflects capture of magma ascending beneath the south Tonga arc. The average field density for surveyed sections of the Tonga-Kermadec arc is comparable to that of surveyed MORs in the eastern Pacific.

[44] 3. The maximum values for several hydrothermal tracers (ΔpH, H_2S, PS, Fe, and Mn) were generally lower on the south Tonga arc compared to those reported for the Kermadec arc. However, large excursions in plume pH were observed at

multiple sites on the south Tonga arc, indicating venting of magmatic volatiles such as CO_2, SO_2, and H_2S. With the exception of a high concentration of PS in the Mariner plume, indications of volatile discharge (e.g., anomalies in δ^3He, pH, and CH_4) on the VFR were generally less intense than on the south Tonga arc.

[45] 4. Accumulations of ^{3}He, Fe, and Mn within the deep, south Lau Basin (*TELVE* study area) appear to result from venting on the VFR. The efficient extraction of Fe and Mn from the subseafloor at the Mariner site (as evidenced by high Fe/heat and Mn/heat values compared to MOR systems) is a major contributor of this Fe and Mn.

[46] 5. On the basis of a comparison of site density and plume chemical intensity for (Fe + Mn) along large sections of the convergent (intraoceanic arcs) and divergent (MORs) margins of the Pacific plate, we suggest that a significant fraction of the total hydrothermal input for these metals to the Pacific basin may occur from submarine arcs. The chemical discharge from arcs is particularly well suited to directly influence the surface ocean, where processes such as primary production may be stimulated by additions of hydrothermal Fe.

Acknowledgments

[47] This research was supported by the Mineral Wealth of New Zealand and its Exclusive Economic Zone program funded by the New Zealand Foundation for Research and Technology (FRST) and the NOAA VENTS and Ocean Exploration Programs. We thank the officers and crew of the R/V *Southern Surveyor* and Rennie Vaiomo'unga, Ministry of Lands, Tonga, for onboard assistance. David Christie and Charlotte Goddard shared geochemical data for lavas collected during *TELVE*. PMEL contribution 2979.

References

Baker, E. T., and C. R. German (2004), On the global distribution of hydrothermal vent fields, in *Mid-Ocean Ridges: Hydrothermal Interactions Between the Lithosphere and Oceans*, *Geophys. Monogr. Ser.*, vol. 148, edited by C. R. German, J. Lin, and L. M. Parson, pp. 245–266, AGU, Washington, D. C.

Baker, E. T., D. A. Tennant, R. A. Feely, G. T. Lebon, and S. L. Walker (2001), Field and laboratory studies on the effect of particle size and composition on optical backscattering measurements in hydrothermal plumes, *Deep Sea Res., Part I*, *48*, 593–604.

Baker, E. T., et al. (2002), Hydrothermal venting along Earth's fastest spreading center: East Pacific Rise, 27.5°–32.3°, *J. Geophys. Res.*, *107*(B7), 2130, doi:10.1029/2001JB000651.

Baker, E. T., R. A. Feely, C. E. J. de Ronde, G. J. Massoth, and I. C. Wright (2003), Submarine hydrothermal venting on the southern Kermadec volcanic arc front (offshore New Zealand): Location and extent of particle plume signatures, in *Intra-Oceanic Subduction Systems: Tectonic and Magmatic Processes*, edited by R. D. Larter and P. T. Leat, *Geological Soc. Spec. Publ.*, *219*, 141–161.

Baker, E. T., G. J. Massoth, K. Nakamura, R. W. Embley, C. E. J. de Ronde, and R. J. Arculus (2005), Hydrothermal activity on near-arc sections of back-arc ridges: Results from the Mariana Trough and Lau Basin, *Geochem. Geophys. Geosyst.*, *6*, Q09001, doi:10.1029/2005GC000948.

Baker, E. T., J. A. Resing, S. L. Walker, F. Martinez, B. Taylor, and K. Nakamura (2006), Abundant hydrothermal venting along melt-rich and melt-free ridge segments in the Lau back-arc basin, *Geophys. Res. Lett.*, *33*, L07308, doi:10.1029/2005GL025283.

Bevis, M., et al. (1995), Geodetic observations of very rapid convergence and back-arc extension at the Tonga arc, *Nature*, *374*, 249–251.

Bloomer, S. H., A. Ewart, J. M. Hergt, and W. B. Bryan (1994), Geochemistry and origin of igneous rocks from the outer Tonga forearc (Site 841), *Proc. Ocean Drill. Program Sci. Results*, *135*, 625–646.

Bostrom, K., and M. N. A. Peterson (1966), Precipitates from hydrothermal exhalations on the East Pacific Rise, *Econ. Geol.*, *61*, 1258–1265.

Boyd, P. W., et al. (2000), A mesoscale phytoplankton bloom in the polar Southern Ocean stimulated by iron fertilization, *Nature*, *407*, 695–702.

Boyle, E. A., B. A. Bergquist, R. A. Kayser, and N. Mahowald (2005), Iron, manganese, and lead at Hawaii Ocean Time-series station Aloha: Temporal variability and an intermediate water hydrothermal plume, *Geochim. Cosmochim. Acta*, *64*(4), 933–952.

Cañón-Tapia, E., and G. P. L. Walker (2004), Global aspects of volcanism: The perspectives of "plate tectonics" and "volcanic systems,", *Earth Sci. Rev.*, *66*, 163–182.

Coale, K. H., S. E. Fitzwater, R. M. Gordon, K. S. Johnson, and R. T. Barber (1996), Control of community growth and export production by upwelled iron in the equatorial Pacific Ocean, *Nature*, *379*, 621–624.

Collier, J. S., and M. C. Sinha (1990), Seismic images of a magma chamber beneath the Lau Basin back-arc spreading centre, *Nature*, *346*, 646–648.

Collier, J. S., and M. C. Sinha (1992), The Valu Fa Ridge: The pattern of volcanic activity at a back-arc spreading centre, *Mar. Geol.*, *104*, 243–263.

Cowen, J. P., G. J. Massoth, and R. A. Feely (1990), Scavenging rates of dissolved manganese in a hydrothermal vent plume, *Deep Sea Res., Part A*, *37*(10), 1619–1637.

Cronan, D. S., and R. A. Hodkinson (1997), Geochemistry of hydrothermal sediments from ODP sites 834 and 834 in the Lau Basin, Southwest Pacific, *Mar. Geol.*, *141*, 237–268.

Daesslé, L. W., D. S. Cronan, V. Marchig, and M. Wiedicke (2000), Hydrothermal sedimentation adjacent to the propagating Valu Fa Ridge, Lau Basin, SW Pacific, *Mar. Geol.*, *162*, 479–500.

Day, A. J., C. Peirce, and M. C. Sinha (2001), Three-dimensional crustal structure and magma chamber geometry at the intermediate-spreading, back-arc Valu Fa Ridge, Lau Basin: Results of a wide-angle seismic tomographic inversion, *Geophys. J. Int.*, *146*, 31–52.

de Ronde, C. E. J., E. T. Baker, G. J. Massoth, J. E. Lupton, I. C. Wright, R. A. Feely, and R. R. Greene (2001), Intra-oceanic subduction-related hydrothermal venting, Kermadec volcanic arc, New Zealand, *Earth Planet. Sci. Lett.*, *193*, 359–369.

de Ronde, C. E. J., G. J. Massoth, E. T. Baker, and J. E. Lupton (2003), Submarine hydrothermal venting related to volcanic arcs, *Soc. Econ. Geol. Spec. Publ.*, *10*, 91–110.

de Ronde, C. E. J., et al. (2005), Evolution of a submarine magmatic-hydrothermal system: Brothers volcano, southern Kermadec arc, New Zealand, *Econ. Geol.*, *100*, 1097–1133.

de Ronde, C. E. J., et al. (2007), Submarine hydrothermal activity along the mid-Kermadec Arc, New Zealand: Large-scale effects on venting, *Geochem. Geophys. Geosyst.*, *8*, Q07007, doi:10.1029/2006GC001495.

Embley, R. W., et al. (1998), Geological, chemical, and biological evidence for recent volcanism at 17.5°S: East Pacific Rise, *Earth Planet. Sci. Lett.*, *163*, 131–147.

Embley, R. W., E. T. Baker, W. W. Chadwick Jr., J. E. Lupton, J. A. Resing, G. J. Massoth, and K. Nakamura (2004), Exploration of Marina Arc volcanoes reveal new hydrothermal systems*Eos Trans. AGU*, *85*, 37–40.

Embley, R. W., et al. (2006), Long-term eruptive activity at a submarine arc volcano, *Nature*, *441*, 494–497, doi:10.1038/nature04762.

Feely, R. A., G. J. Massoth, and G. T. Lebon (1991), Sampling of marine particulate matter and analysis by x-ray fluorescence spectrometry, in *Marine Particles: Analysis and Characterization*, *Geophys. Monogr. Ser.*, vol. 63, edited by D. C. Hurd and D. W. Spencer, pp. 251–257, AGU, Washington, D. C.

Feely, R. A., J. F. Gendron, E. T. Baker, and G. T. Lebon (1994), Hydrothermal plumes along the East Pacific Rise, 8°40′ to 11°50′N: Particle distribution and composition, *Earth Planet. Sci. Lett.*, *128*, 19–36.

Field, M. P., and R. M. Sherrell (2000), Dissolved and particulate Fe in a hydrothermal plume at 9°45′N, East Pacific Rise: Slow Fe (II) oxidation kinetics in Pacific plumes, *Geochim. Cosmochim. Acta*, *64*, 619–628.

Fouquet, Y., et al. (1991a), Hydrothermal activity and metallogenesis in the Lau back-arc basin, *Nature*, *349*, 778–781.

Fouquet, Y., U. von Stackelberg, J.-L. Charlou, J. Ersinger, P. Herzig, R. Mühe, M. Wiedicke, S. Soakai, and H. Whitechurch (1991b), Hydrothermal activity in the Lau back-arc basin: Sulfides and water chemistry, *Geology*, *19*, 303–306.

Fouquet, Y., U. von Stackelberg, J.-L. Charlou, J. Erzinger, P. M. Herzig, R. Mühe, and M. Wiedicke (1993), Metallogenesis in back-arc environments: The Lau Basin example, *Econ. Geol.*, *88*, 2154–2181.

Fretzdorff, S., U. Schwarz-Schampera, H. L. Gibson, C.-D. Garbe-Schönberg, F. Hauff, and P. Stoffers (2006), Hydrothermal activity and magma genesis along a propagating back-arc basin: Valu Fa Ridge (southern Lau Basin), *J. Geophys. Res.*, *111*, B08205, doi:10.1029/2005JB003967.

Hannington, M. D., de C. E. J. Ronde, and S. Petersen (2005), Modern sea-floor tectonics and submarine hydrothermal systems, in *Economic Geology 100th Anniversary Volume*, edited by J. W. Hedenquist et al., pp. 111–141, Soc. of Econ. Geol., Littleton, Colo.

Harding, A. J., G. M. Kent, and J. A. Collins (2000), Initial results from a multichannel seismic survey of the Lau back-arc basin, *Eos Trans. AGU*, *81*(48), Fall Meet. Suppl., Abstract T61C-16.

Hawkins, J. W. (1995), Evolution of the Lau Basin—Insights from ODP Leg 135, in *Active Margins and Marginal Basins of the Western Pacific*, *Geophys. Monogr. Ser.*, vol. 88, edited by B. Taylor and J. Natland, pp. 125–173, AGU, Washington, D. C.

Hein, J. R., M. S. Schulz, and J.-K. Kang (1990), Insular and submarine ferromanganese mineralization of the Tonga-Lau region, *Mar. Min.*, *9*, 305–354.

Hilton, D. R., T. P. Fischer, and B. Marty (2002), Noble gases and volatile recycling at subduction zones, *Rev. Mineral. Geochem.*, *47*, 319–370.

Ishibashi, J., H. Wakita, K. Okamura, E. Nakayama, R. A. Feely, G. T. Lebon, E. T. Baker, and K. Marumo (1997), Hydrothermal methane and manganese variation in the plume of the superfast-spreading southern East Pacific Rise, *Geochim. Cosmochim. Acta*, *61*(3), 485–500.

Ishibashi, J., J. E. Lupton, T. Yamaguchi, J. Querellou, T. Nunoura, and K. Takai (2006), Expedition reveals changes in Lau Basin hydrothermal system, *Eos Trans. AGU*, *87*(2), 13–24.

Klinkhammer, G. P., and M. L. Bender (1980), The distribution of manganese in the Pacific Ocean, *Earth Planet. Sci. Lett.*, *46*, 361–384.

Lupton, J. E. (1990), Water column hydrothermal plumes on the Juan de Fuca Ridge, *J. Geophys. Res.*, *95*(B8), 12,829–12,842.

Lupton, J. E., G. P. Klinkhammer, W. R. Normark, R. Haymon, K. C. Macdonald, R. F. Weiss, and H. Craig (1980), Helium-3 and manganese at the 21°N East Pacific Rise hydrothermal site, *Earth Planet. Sci. Lett.*, *50*, 115–127.

Lupton, J. E., E. T. Baker, M. J. Mottl, F. J. Sansone, C. G. Wheat, J. A. Resing, G. J. Massoth, C. I. Measures, and R. A. Feely (1993), Chemical and physical diversity of hydrothermal plumes along the East Pacific Rise, 8°45′N to 11°50′N, *Geophys. Res. Lett.*, *20*(24), 2913–2916.

Lupton, J. E., D. G. Pyle, W. J. Jenkins, R. Greene, and L. Evans (2004), Evidence for an extensive hydrothermal plume in the Tonga-Fiji region of the South Pacific, *Geochem. Geophys. Geosyst.*, *5*, Q01003, doi:10.1029/2003GC000607.

Lupton, J., et al. (2006), Submarine venting of liquid carbon dioxide on a Mariana Arc volcano, *Geochem. Geophys. Geosyst.*, *7*, Q08007, doi:10.1029/2005GC001152.

Malahoff, A., I. Ya. Kolotyrkina, B. P. Midson, and G. J. Massoth (2006), A decade of exploring a submarine intraplate volcano: Hydrothermal manganese and iron at Lo'ihi volcano, Hawai'i, *Geochem. Geophys. Geosyst.*, *7*, Q06002, doi:10.1029/2005GC001222.

Martinez, F., and B. Taylor (2002), Mantle wedge control on back-arc crustal accretion, *Nature*, *416*, 417–420.

Martinez, F., and B. Taylor (2003), Controls on back-arc crustal accretion: Insights from the Lau, Manus and Marina basins, in *Intra-Oceanic Subduction Systems: Tectonic and Magmatic Processes*, edited by R. D. Larter and P. T. Leat, *Spec. Publ. Geol. Soc.*, *219*, 19–54.

Martinez, F., B. Taylor, E. T. Baker, J. A. Resing, and S. L. Walker (2006), Opposing trends in crustal thickness and spreading rate along the back-arc Eastern Lau Spreading Center: Implications for controls on ridge morphology, faulting, and hydrothermal activity, *Earth Planet. Sci. Lett.*, *245*, 655–672.

Massoth, G. J., and R. N. Hey (1998), SUAVE perspectives on the Southern East Pacific Rise, *Eos Trans. AGU*, *79*(45), Fall Meet. Suppl., F831.

Massoth, G. J., E. T. Baker, J. E. Lupton, R. A. Feely, D. A. Butterfield, K. L. Von Damm, K. K. Roe, and G. T. Lebon (1994), Temporal and spatial variability of hydrothermal manganese and iron at Cleft segment, Juan de Fuca Ridge, *J. Geophys. Res.*, *99*(B3), 4905–4923.

Massoth, G. J., E. T. Baker, R. A. Feely, J. E. Lupton, R. W. Collier, J. F. Gendron, K. K. Roe, S. M. Maenner, and J. A. Resing (1998), Manganese and iron in hydrothermal plumes resulting from the 1996 Gorda Ridge event, *Deep Sea Res., Part II*, *45*, 2683–2712.

Massoth, G. J., C. E. J. de Ronde, J. E. Lupton, R. A. Feely, E. T. Baker, G. T. Lebon, and S. M. Maenner (2003), Chemically rich and diverse submarine hydrothermal plumes of the southern Kermadec volcanic arc (New Zealand), in *Intra-Oceanic Subduction Systems: Tectonic and Magmatic Processes*, edited by R. D. Larter and P. T. Leat, *Spec. Publ. Geol. Soc.*, *219*, 119–139.

Massoth, G. J., et al. (2005), Plume-vent fluid connections along the Tonga-Kermadec arc, *Eos Trans. AGU*, *86*(49), Fall Meet. Suppl., Abstract V44A-04.

Measures, C., J. Yuan, and J. Resing (1995), Determination of iron in seawater by flow injection analysis using in-line preconcentration and specrophotometric detection, *Mar. Chem.*, *50*, 3–12.

Morton, J. L., and N. H. Sleep (1985), A mid-ocean ridge thermal model: Constraints on the volume of axial hydrothermal heat, *J. Geophys. Res.*, *90*, 11,345–11,353.

Mottl, M. J., F. J. Sansone, C. G. Wheat, J. A. Resing, E. T. Baker, and J. E. Lupton (1995), Manganese and methane in hydrothermal plumes along the East Pacific Rise, 8°40′ to 11°50′N, *Geochim. Cosmochim. Acta*, *59*(20), 4147–4165.

Resing, J. A., and M. J. Mottl (1992), Determination of manganese in seawater by flow injection analysis using on-line preconcentration and spectrophotometric detection, *Anal. Chem.*, *64*, 2682–2687.

Resing, J. A., R. A. Feely, G. J. Massoth, and E. T. Baker (1999), The water-column chemical signature after the 1998 eruption of Axial Volcano, *Geophys. Res. Lett.*, *26*, 3645–3648.

Resing, J. A., G. Lebon, E. Baker, J. Lupton, K. Nakamura, G. Massoth, and R. Embley (2003), Geochemical characterization of hydrothermal plumes above hydrothermally active volcanoes on the Mariana arc, *Eos Trans. AGU*, *84*(46), Fall Meet. Suppl., Abstract T32A-0915.

Resing, J. A., J. E. Lupton, R. A. Feely, and M. D. Lilley (2004), CO_2 and ^3He in hydrothermal plumes: Implications for mid-ocean ridge CO_2 flux, *Earth Planet. Sci. Lett.*, *226*, 449–464.

Sakamoto-Arnold, C. M., K. S. Johnson, and C. L. Beehler (1986), Determination of hydrogen sulfide in seawater using flow-injection analysis and flow analysis, *Limonol. Oceanogr.*, *31*, 894–900.

Seewald, J., et al. (2005), Aqueous volatilities in Lau Basin hydrothermal fluids, *Eos Trans. AGU*, *86*(49), Fall Meet. Suppl., Abstract T31A-0478.

Sharkey, J., G. C. Wheat, M. J. Mottl, and J. Seewald (2005), Vent fluid chemistry from six hydrothermal fields along the Eastern Lau spreading center from 20°03′S to 22°13′S, *Eos Trans. AGU*, *86*(49), Fall Meet. Suppl., Abstract T31A-0479.

Stanton, R. I. (1994), *Ore Elements in Arc Lavas*, *Oxford Monogr. Geol. Geophys.*, vol. 29, Oxford Univ. Press, New York.

Stoffers, P., et al. (2003), Cruise Report Sonne 167, Louisville Ridge: Dynamics and magmatism of a mantle plume and its influence on the Tonga-Kermadec subduction system, Suva, Fiji–Wellington, New Zealand, 12 October–02 December 2002: Berichte–Reports, *20*, 276 pp., Inst. für Geowiss., Univ. Kiel, Kiel, Germany.

Stoffers, P., et al. (2006), Submarine volcanoes and high-temperature hydrothermal venting on the Tonga arc, southwest Pacific, *Geology*, *34*, 453–456.

Tachibana, K., A. Hattori, M. Yokoi, T. Kodachi, and N. Asaoka (1991), For practical use of a system for determining pH's of high-temperature aqueous solutions. 1. Preparation of ZrO_2 membrane tubes and a pressure balanced regulator, *Corrosion Eng.*, *40*, 365–377.

Taylor, B., and F. Martinez (2003), Back-arc basin basalt systematics, *Earth Planet. Sci. Lett.*, *210*, 481–497.

Tivey, M. K., et al. (2005), Characterization of six vent fields within the Lau Basin, *Eos Trans. AGU*, *86*(49), Fall Meet. Suppl., Abstract T31A-0477.

Turner, I. M., C. Peirce, and M. C. Sinha (1999), Seismic imaging of the axial region of the Valu Fa Ridge, Lau Basin: The acretionary processes of an intermediate back-arc spreading ridge, *Geophys. J. Int.*, *138*, 495–519.

von Stackelberg, U., and the Shipboard Scientific Party (1988), Active hydrothermalism in the Lau back-arc basin (SW Pacific): First results from the SONNE 48 Cruise, (1987), *Mar. Min.*, *7*, 431–442.

Wells, M. L., G. K. Vallis, and E. A. Silver (1999), Tectonic processes in Papua New Guinea and past productivity in the eastern equatorial Pacific Ocean, *Nature*, *398*, 601–604.

Wiedicke, M., and J. Collier (1993), Morphology of the Valu Fa spreading ridge in the southern Lau Basin, *J. Geophys. Res.*, *98*(B7), 11,769–11,782.

Wright, D. J., S. H. Bloomer, C. J. MacLeod, B. Taylor, and A. M. Goodlife (2000), Bathymetry of the Tonga Trench and Forearc: A map series, *Mar. Geophys. Res.*, *21*, 489–511.

Young, C., and J. E. Lupton (1983), An ultra-tight fluid sampling system using cold-welded copper tubing, *Eos Trans. AGU*, *64*, 735.

Zellmer, K. E., and B. Taylor (2001), A three-plate kinematic model for Lau Basin opening, *Geochem. Geophys. Geosyst.*, *2*(5), doi:10.1029/2000GC000106.